

A CENTER OF COMPETENCE IN SOLID STATE MATERIALS AND DEVICES

by

Fred A. Lindholm, Arthur J. Brodersen, Eugene R. Chenette, Robert W. Gould,
Larry L. Hench, John J. Hren, Sheng S. Li, James K. Watson

College of Engineering
University of Florida
Gainesville, Florida 32601

Contract No. F 19628-68-C-0058

Project No. 8687

Electrical Engineering Department

Scientific Report No. 1

10 April 1968

Contract Monitor

Richard F. Cornelissen
Solid State Sciences Laboratory

Distribution of this document is unlimited. It may be released to the Clearinghouse, Department of Commerce, for sale to the general public.

Prepared for

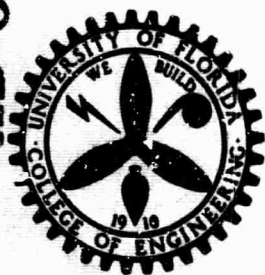
**AIR FORCE CAMBRIDGE RESEARCH LABORATORIES
OFFICE OF AEROSPACE RESEARCH
UNITED STATES AIR FORCE
BEDFORD, MASSACHUSETTS**

DDC
RECEIVED
JUN 4 1968
RECEIVED
B

This research was supported by the Advanced Research Projects Agency under ARPA Order No. 1060

Reproduced by the
CLEARINGHOUSE
for Federal Scientific & Technical
Information Springfield Va. 22151

AD 669580



AFCRL-68-0185

A CENTER OF COMPETENCE IN SOLID STATE MATERIALS AND DEVICES

by

Fred A. Lindholm, Arthur J. Brodersen, Eugene R. Chenette, Robert W. Gould,
Larry L. Hench, John J. Hren, Sheng S. Li, James K. Watson

College of Engineering
University of Florida
Gainesville, Florida 32601

Contract No. F 19628-68-C-0058

Project No. 8687

Electrical Engineering Department

Scientific Report No. 1

10 April 1968

Contract Monitor
Richard F. Cornelissen
Solid State Sciences Laboratory

Distribution of this document is unlimited. It may be
released to the Clearinghouse, Department of Commerce,
for sale to the general public.

Prepared
for

**AIR FORCE CAMBRIDGE RESEARCH LABORATORIES
OFFICE OF AEROSPACE RESEARCH
UNITED STATES AIR FORCE
BEDFORD, MASSACHUSETTS**

This research was supported by the Advanced Research Projects Agency
under ARPA Order No. 1060

BLANK PAGE

ABSTRACT

This report, for the first semiannual period of contract support, describes technical findings concerned with glass-ceramic dielectrics, semiconducting glasses, electronic and structural properties of semiconductors, near-degenerate pn junctions, and radiation studies on materials. In addition to the reporting of these technical findings, major additions to our experimental capability made during this period are summarized.

Two detailed reportings are made concerning structure in glass-ceramic dielectrics: one concerning the kinetics of crystallization, studied by quantitative x-ray diffraction, and the other concerning structural changes resulting from thermal treatment, studied by electron microscopy, x-ray analysis, and dc and ac electrical properties. For semiconducting glasses, correlations are made concerning thermal treatment and structural changes, on the one hand, and dielectric and electronic properties, on the other. Results are reported from two studies aimed toward determining the structure of compound and elemental semiconductors. An expression for the diffusivity-mobility ratio is derived that is valid for degenerate as well as non-degenerate semiconductors, and is used to plot this ratio against carrier concentration. Brief disclosure is made concerning the radiation stability of semiconducting glasses and insulating glass-ceramics.

SUMMARY

The general objective of this research program is to establish at the University of Florida a center of competence in unconventional solid-state materials and devices. In accord with this general objective, research studies are to be undertaken in three areas: first, the study of solid-state materials not used in the present technology of silicon integrated circuits; second, the study of properties of silicon the understanding of which is lacking yet important for device design; third, the exploitation of these studies in the creation of new devices and circuits. Potential D.O.D. applications in the areas of detection, navigation, surveillance, and control will guide the choice of materials to be studied and device applications to be considered. (Section I of this report discusses the plans and objectives of the research program in detail.)

This report, for the first semi-annual period of contract support, describes technical findings concerned with glass-ceramic dielectrics, semiconducting glasses, electronic and structural properties of semiconductors, near-degenerate pn junctions, and radiation studies on materials. In addition to the reporting of these technical findings, major additions to our experimental capability made during this period are summarized.

Detailed accounts are given of two studies dealing with structural changes in glass-ceramic dielectrics. The first study concerns the kinetics of crystallization of $\text{Li}_2\text{Si}_2\text{O}_5$ from glasses in the $\text{Li}_2\text{O}-\text{SiO}_2$ system, studied by quantitative x-ray diffraction. Analysis of the data analysed using the Johnson-Mehl-Avrami equation showed that crystallization occurred through the nucleation and growth of rods. The spherulitic nature of the crystals was substantiated by petrographic examinations of the partially crystalline glass. Analysis of the temperature dependence of the crystallization rate using a modification of the Johnson-Mehl-Avrami equation showed that the activation energy for nucleation was

a function of composition and thermal treatment.

The second study deals with glass structural differences in a 17.5 weight % $\text{Li}_2\text{O-SiO}_2$ glass resulting from thermal treatments in the annealing-transformation range. These were studied using electron microscopy, x-ray analysis, and dc and ac electrical properties. It was shown that metastable crystalline lithium metasilicate precipitates and subsequently redissolves prior to the appearance of the equilibrium lithium disilicate crystals. The lithium metasilicate gives rise to dielectric loss peaks in the 100 Hz to 1 MHz range; the Maxwell-Wagner-Sillars heterogeneous dielectric model is used to justify this observation.

For semiconducting glasses, correlations have been made concerning thermal treatment and structural changes, on the one hand, and dielectric and electronic properties, on the other. These are briefly reported, as are results from two studies relevant to determining aspects of the structure of elemental and compound semiconductors: (1) a computer simulation of surface defects in diamond cubic structures, which is intended to aid in the quantitative interpretation of field-ion-microscope images of many semiconductors; (2) preliminary data, yielded by small-angle x-ray scattering, related to the clustering of impurity atoms in degenerate silicon. Brief disclosure is also made of some tentative theoretical expressions describing the behavior of near-degenerate pn junctions and of the radiation stability of semiconducting glasses and insulating glass-ceramics.

An expression has been derived, formulated in terms of tabulated functions, for a generalized Einstein relation valid for degenerate as well as non-degenerate semiconductors. To facilitate the use of this expression in device design, a graph has been constructed displaying the diffusivity-mobility ratio against carrier concentration; the graph holds for any temperature and for any material whose density of quantum states varies, to a reasonable approxi-

mation, as the square root of energy. Separate curves have been plotted for the special cases of silicon and germanium. For any level of concentration, these curves afford a comparison with the constant value of the diffusivity-mobility ratio predicted by the conventional Einstein relation, and display the error deriving from its misuse. For holes in silicon, as an example, the conventional relation starts to fail at a concentration of approximately $4 \times 10^{18} \text{ cm}^{-3}$; at a density of 10^{19} cm^{-3} , at which the Fermi level approximately coincides with the band edge, the error introduced is about 40 per cent; at a density of $2 \times 10^{20} \text{ cm}^{-3}$, the error exceeds a factor of five.

Improvements in experimental capability that were made during this period include an important modification of the electron microprobe and significant progress in the development of the laboratory for noise studies and of the magnetic-film laboratory. Moreover, the solid-state fabrication laboratory is now available as a research tool. In illustration of its capability, successive runs yielded good bipolar transistors with Betas exceeding fifty; all processing, from mask-making and photolithography through diffusions and metallization, were done in the laboratory.

TABLE OF CONTENTS

	<u>Page</u>
Summary	ii
I. Introduction	1
II. Glass-Ceramic Dielectrics and Glass Semiconductors (L.L. Hench)	3
A. The Kinetics of Crystallization in $\text{Li}_2\text{O-SiO}_2$ Glasses	5
B. Effect of a Metastable Precipitate on the Electrical Properties of a $\text{Li}_2\text{O-SiO}_2$ Glass	25
III. Semiconductors and Semiconducting Devices (F.A. Lindholm, S.S. Li, R.W. Gould, J.J. Hren, L.L. Hench, E.R. Chenette, C.T. Sah)	48
A. Generalized Einstein Relation for Degenerate Semiconductors (F.A. Lindholm, S.S. Li)	50
B. Computer Simulation of Surface Defects in Diamond Cubic Structures: Dislocations Intersecting a Surface (J.J. Hren)	60
C. Distribution of Solute Elements in Degenerate Semiconductors (R.W. Gould)	63
D. Toward a Theory of Near-Degenerate PN Junctions (F.A. Lindholm)	67
IV. Radiation Studies (L.L. Hench)	69
V. Noise Studies (E.R. Chenette, A.J. Brodersen)	74
VI. Laboratory Facilities	76
A. Solid-State Fabrication Laboratory (A.J. Brodersen)	76
B. Modification of Electron Microscope (R.W. Gould)	80
C. Magnetic Film Laboratory (J.K. Watson; assisted by R.G. Singh)	87
VII. Discussion	90

BLANK PAGE

1. INTRODUCTION

The general objective of this research program is to establish at the University of Florida a center of competence in unconventional solid-state materials and devices. In accord with this general objective, the research is to seek:

1. A basic understanding and characterization of materials not presently used in the silicon technology. The materials to be studied include insulators, metals and semiconductors (both single-crystal and polycrystalline) that have potential use in solid-state devices.
2. A basic and precise understanding and characterization of those properties of silicon that have high potential importance in device design and yet have not received attention in either industrial, governmental, or university research.
3. A basic understanding and characterization of materials exposed to high-radiation environments or environments involving extremes in temperature.
4. The utilization of the acquired understanding of materials to create new devices and circuits that involve materials and principles not used presently in the conventional technology.
5. The demonstration of the usefulness of the new devices and circuits by testing their applicability in the solution of representative equipment and application problems in the areas of detection, surveillance, navigation, and control.

The research will seek to correlate the structural parameters of each material under study with its electronic and quantum parameters. Further correlation will be sought to determine the variations in the structural, electronic, and quantum parameters that result from irradiation. Having established these correlations, the research staff will then utilize our fabrication facilities, attempting to determine changes in processing that will yield better materials for each envisioned device application.

During this first six months of contract support, the two Departments principally responsible for this research, the Electrical Engineering Department and the Metallurgical and Materials Engineering Department began

moves into new buildings. These moves, and the attendant establishment or re-establishment of equipment relevant to this research program, have been completed. Moreover, the research team has made good progress in other tasks that necessarily precede the undertaking of the actual research - such tasks as the design of experiments, the ordering and installing of equipment, and the acquisition and training of support personnel. All of these efforts have consumed a considerable portion of the time available to the research team.

In Sections V and VI, therefore, this first report will describe briefly some of the results of this effort, concentrating on major additions to our experimental capability made during this first six-month period. The major part of this report, however, describes specific technical findings. These appear in Sections II through IV.

II. Glass-Ceramic Dielectrics and Glass Semiconductors (L. L. Hench)

Semiconducting Glasses

Hamblen¹ has reported that partially crystallized semiconducting glass compositions possess much larger D.C. conductivities than the quenched glasses. Hench and Jenkins² have demonstrated interesting A.C. properties in quenched semiconducting glasses of similar $V_2O_5-P_2O_5$ compositions. Hench and Daughenbaugh³ have shown that the D.C. conductivity and A.C. behavior of several vanadia-phosphate glasses are stable to neutron dosages of 4×10^{17} nvt and γ -ray doses of 1.2×10^8 rads.

The objective of the present program is to investigate the sequence of structural changes that accompany the thermal treatment of a semiconducting glass and relate the changes in electrical properties to structure. Several important observations have been made in this area and papers are being prepared for publication. Heterogeneous dielectric loss peaks have been discovered in the partially crystallized glasses, and they have been rationalized in terms of a Maxwell-Wagner-Sillars model⁴. Decreases in D.C. resistivity from 10^9 ohm-cm to 10^2 ohm-cm have been attributed to the development of crystals in the glass by either isothermal heat treatments or variations in quenching temperatures⁵. As the mean free path between crystals in the glass decreases the frequency-enhanced conductivity characteristic of a semiconducting glass disappears.⁵

Theoretical analysis of the conduction mechanism of semiconducting glasses is in progress. The model basically consists of frequency assisted polaron hopping between localized energy states in the glass. The influence of A.C. fields, regions of ordered non-localized states, compositional changes and irradiation effects are being quantitatively examined in terms

of the model.

REFERENCES

1. D.P. Hamblen, R.A. Weidel, G.E. Blair, J. Am. Ceram. Soc. **46**, 499 (1963)
2. L.L. Hench and D.A. Jenkins, Phys. Stat. Sol. **20**, 327 (1967).
3. L.L. Hench and G.A. Daughenbaugh, "Radiation Effects in Glass Semiconductors," J. Nuclear Materials, in press.
4. L.L. Hench, A.E. Clark, D.L. Kinser, "Heterogeneous Dielectric Losses in a Semiconducting Glass," to be submitted to J. Electrochem. Soc.
5. L.L. Hench, A.E. Clark, D.L. Kinser, "Electrical Properties of a Thermally Treated Semiconducting Glass," to be submitted to J. Am. Ceram. Soc.

Glass Ceramics

The objective of the glass-ceramic research program is to obtain an understanding of the influence of structure on the electrical, mechanical and thermal properties of this class of materials. Attention is concentrated on binary lithia-silicate and soda-silicate glasses in order to simplify structural interpretation.

The emphasis of the program in this report has been devoted to two studies of structural changes.

First, we report on the kinetics of crystallization of $\text{Li}_2\text{O-SiO}_2$ glasses with various nucleation treatments. (This work has formed the basis of a paper, by S.W. Freiman and L. L. Hench, accepted for publication by the Journal of the American Ceramic Society.) Second, we report on structural changes occurring in thermally treated $\text{Li}_2\text{O-SiO}_2$ glasses analysed by dielectric absorption and x-ray Guinier analysis. (This work has formed the basis of a paper, by D.L. Kinser and L.L. Hench, accepted for publication by the Journal of the American Ceramic Society.)

A. THE KINETICS OF CRYSTALLIZATION IN $\text{Li}_2\text{O}-\text{SiO}_2$ GLASSES

Introduction

Previous investigations of the growth of $\text{Li}_2\text{Si}_2\text{O}_5$ crystals in $\text{Li}_2\text{O}-\text{SiO}_2$ glasses¹⁻² and of the kinetics of bulk crystallization, involving a combination of both nucleation and growth, in $\text{Li}_2\text{O}-\text{SiO}_2$ glasses³⁻⁴ have been reported. A summary of the experimental methods, glass compositions, and results of the earlier studies is presented in Table I. There appears to be agreement on an activation energy of 56 Kcal/mole for the growth of $\text{Li}_2\text{Si}_2\text{O}_5$ crystals. However, the activation energies of bulk crystallization obtained from the various experiments differ by as much as a factor of 2.4.

The objective of the present investigation was to resolve these differences by determining the effect of composition and nucleation treatments on the activation energy and the rate of crystallization of $\text{Li}_2\text{Si}_2\text{O}_5$ from glasses in the $\text{Li}_2\text{O}-\text{SiO}_2$ system. A second purpose was to show that the Johnson-Mehl-Avrami (JMA) equation could be effectively used to analyze crystallization in glasses when nucleation and growth occur simultaneously.

Experimental Procedure

The samples were prepared from five micron MinUSil^{*} SiO_2 , reagent grade Li_2CO_3 ,^{**} and reagent grade TiO_2 . Three glass compositions were prepared, $\text{SiO}_2 + 33.3$ mole % Li_2O (samples A and C), $(\text{SiO}_2 + 33.3$ mole % $\text{Li}_2\text{O}) + 3.7$ mole % TiO_2 (sample B), and $\text{SiO}_2 + 25$ mole % Li_2O (sample D). The methods of analysis, melting temperatures, and nucleation heat treatments for these samples are given in Table II. The glasses were melted in a covered Pt. crucible. The melts were held at temperature from 18 to 70 hours in order to

* Trademark of the Pennsylvania Glass and Sand Company.

** Supplied by Foote Mineral Company.

completely homogenize the glass. The shorter times were used after it was found that the longer refining times had no effect on the crystallization kinetics.

The glasses were cast as cylinders 2.5 cm long and 1.3 cm in diameter. In order to eliminate scatter in the crystallization data, the crucible was returned to the furnace and reheated to the melting temperature after each specimen was cast. Each specimen was heat treated for 4 hours at 230°C in order to reduce the stresses to a level sufficient to prevent sample breakage. Samples A, B, and C were completely clear, but sample D was bluish indicating that phase separation had already occurred. This general behavior is consistent with the observations of Porai-Koshits and Aver'yanov,⁶ Vogel and Gerth,⁷ and Ohlberg et al.⁸

The heat treatments were performed in a nichrome wound tube furnace containing an aluminum block to eliminate temperature gradients. It was found that if the samples were not given a nucleation heat treatment, primarily surface nucleation occurred, and crystallization within the samples was very nonhomogeneous. The nucleation treatments employed are given in Table II.

Growth temperatures ranged from 549°C to 610°C. Growth times were measured from the time at which the samples reached the desired temperature. This was approximately 20 minutes from the time at which they were placed in the furnace. After the samples were removed from the furnace, they were ground to -200 mesh in a tungsten carbide ball mill. X-ray diffraction specimens were then prepared according to the technique developed by Munch and Pierron.⁹

X-ray diffraction patterns covering a range from 11° to 50° 2 θ were obtained using a Norelco x-ray diffractometer provided with a fine focus Cu

tube and a curved crystal monochromator which was used to reduce the background intensity. The total height of the peaks corresponding to $\text{Li}_2\text{Si}_2\text{O}_5$ in a given sample was compared with the total height of the peaks in a sample which contained 100% crystalline lithium disilicate. Since all of the major peaks of crystalline $\text{Li}_2\text{Si}_2\text{O}_5$ were used to calculate the total diffracted intensity, the effect of preferred orientation of the crystals was eliminated. By analyzing a set of standard samples, it was shown that the ratio of the diffracted intensity from a partially crystalline sample to that from a completely crystalline sample had a one to one correspondence with the weight percent of crystalline phase present. The error in determining percent crystallinity in this manner was $\pm 5\%$. Line broadening observed in the analyses was constant for all samples including the standards, so consequently did not contribute to the analytical error.

Thin sections, approximately 20 microns thick, were prepared from partially crystalline samples. A visual analysis of the crystal morphology was made on these sections by viewing them in transmission under crossed nicols.

Analysis of Volume Percent Crystallization

10-12

Several thermodynamic theories of crystal growth have been developed and recently applied to the growth of $\text{Li}_2\text{Si}_2\text{O}_5$ crystals in $\text{Li}_2\text{O}-\text{SiO}_2$ glasses by Morley.² It is assumed in each of the theories that nucleation of the crystalline phase was completed prior to the onset of crystal growth. However, during the measurement of volume percent crystallization of a glass, nucleation and crystal growth may be occurring simultaneously. This will usually be the case in the heat treatment of a glass unless the Tamman nucleation and growth curves are separated.

The JMA equation¹³⁻¹⁴ has been developed to describe the kinetics of processes where nucleation and growth occur together. The equation has been

used successfully to describe second phase precipitation, eutectoid reactions, and recrystallization in metals. Application of the JMA expression enables one to predict the volume fraction of a new phase that will form as a function of time, if suitable information about the nucleation and growth rates is known or can be assumed.

$$V_V = 1 - \exp \left[- \int_{t'=0}^{t'=1} g l G^n (t-t')^n dt' \right] \quad (1)$$

Equation 1 is the general form of the JMA equation. g is a form factor; G , which is equal to $G_x \cdot G_y \cdot G_z$, is the growth rate; l is the nucleation rate; V_V is the volume fraction of the new phase; t' is the time at which a given particle nucleated; and n is an integer which depends on the dimensionality of the growth mechanism. It can be shown that $n = 3$ for three-dimensional growth of the new phase, $G = G_x \cdot G_y \cdot G_z$ (spheroids). However, $n = 2$ for two-dimensional growth, where $G = G_x \cdot G_y$, $G_z = 0$ (plates, and $n = 1$ for growth in only one dimension, where $G = G_x$, $G_y = 0$, and $G_z = 0$ (rods)).⁵ In Equation 1 the expression $[gG^n(t-t')^n]$ represents the volume at time t of a given particle which nucleated at time t' .

In deriving this equation, the growth rate was assumed to be independent of time. This assumption appears to be valid in the $\text{Li}_2\text{O-SiO}_2$ system based upon Morley's data.²

$$V_V = 1 - \exp \left[- g l G^n t^{n+1} \right] \quad (2)$$

Equation 2 results from the integration of the expression in the exponent in Equation 1. The nucleation rate, l , has been assumed to be independent of time although this assumption is not essential to solving the equation. Equation 3 was obtained from Equation 2 by taking the double logarithm of both sides of the equation.

$$\ln \ln \left(\frac{1}{1-V_V} \right) = (n+1) \ln t + (n+1) \ln (g l G^n) \quad (3)$$

If the temperature dependence of the nucleation and growth rates is included in Equation 2, Equation 4 results:¹⁶

$$V_V = 1 - \exp \left[-gt^{n+1} I_0 e^{-Q_I/RT} (G_0 e^{-Q_G/RT})^n \right] \quad (4)$$

Q_I and Q_G represent the activation energies for nucleation and crystal growth respectively. At constant V_V one obtains Equation 5 by rearranging the terms of Equation 4, and taking the logarithm of both sides:

$$\ln t(V_V) = \frac{Q_I + nQ_G}{(n+1)R} \frac{1}{T} + \frac{\ln G_0^n I_0 \frac{g}{\ln\left(\frac{1}{1-V_V}\right)}}{n+1} \quad (5)$$

It is seen that if the logarithm of the time to form a given volume fraction of crystalline phase is plotted against $1/T$, the slope will be $(Q_I + nQ_G)/[(n+1)R]$.

Results

The percentage of crystallization in the four series of samples is shown as a function of time in Figure 1. The curves for samples B and D were normalized on a basis of the theoretical volume fraction of $\text{Li}_2\text{Si}_2\text{O}_5$ which could be crystallized from each sample. Representative micrographs are shown in Figures 2-4.

The plots of percent crystallization versus time, presented in Figure 1, show that the crystallization rate of $\text{Li}_2\text{Si}_2\text{O}_5$ in this temperature range is decreased by the addition of TiO_2 to 33.3 mole % Li O glass (B), and the appearance of phase separation in the 25 mole % glass (D). However, it can be seen that the crystallization rate is increased when the nucleation time is increased (C). Much of the decrease in overall crystallization rate in

the two cases cited above (B,D) can be attributed to an increase in incubation time, i.e., the time required to form the minimum percent crystallinity detectable by x-ray diffraction, is lengthened.

Most of the samples became hazy a short time before any crystallinity could be detected, suggesting that although some crystals were present, the volume fraction was less than the limit of resolution of the diffractometer.

The logarithm of the time required for the four series of samples to reach 50% crystallization is shown as a function of $1/T$ ($^{\circ}\text{K}$)⁻¹ in Figure 5. It was assumed that spherulitic nucleation and growth began at the time at which crystals were first detected by x-ray diffraction; therefore the zero point was taken to be $V_V = 0$. There is an error introduced in making this assumption since the diffractometer cannot accurately detect volume fractions below approximately 0.05. However, qualitative studies using a Guinier-DeWolff x-ray camera,¹⁷ which can detect crystallinity down to the range of about 0.0001 volume fraction¹⁸ have shown that the $\text{Li}_2\text{Si}_2\text{O}_5$ phase appears very near the time of extrapolation of the x-ray diffraction data. The slopes of the lines in Figure 5 give activation energies for the crystallization process (see also Table II). Comparable values of activation energies were obtained when the temperature dependence of the times to 40% and 60% crystallization were analyzed.

Discussion

As mentioned previously, if the left side of the JMA equation (Equation 3), $\ln \ln [1/(1-V_V)]$, is plotted against $\ln t$, the slope of the line $(n+1)$ indicates the growth morphology of the transforming phase. When the equation was plotted from the point $t = 0$, unrealistically high values of the slope were obtained. If it is assumed that the crystallization rate up to the time at which crystals are first detected is very slow compared to the rate after this time, Equation 3 can be plotted from $V_V = 0$. An example of one of the

graphs obtained is shown in Figure 6. The values of the initial slopes of the curves, before impingement occurs, are presented in Table III. Within experimental error, the values for all of the series are approximately 2, which would be expected if crystal growth during this period is rod-like in nature ($n = 1$), and the nucleation rate is constant ($n + 1 = 2$).

The electronmicrograph of a fracture surface and the photomicrographs made from thin sections (Figures 2-4) support the analytical conclusions that crystal growth occurred in the form of rods and that the nucleation rate was constant. The micrographs of the partially crystallized samples contain spherulitic crystals which are similar to those observed by Matveev and Velya¹⁹, and Korelova et al.²⁰ in this system, and are described generally by Morse and Donnay.²¹ The analyses of Morse and Donnay showed that the increase in size of this form of spherulite occurs through the nucleation and growth of the individual rods that make up the crystals. They proposed that every point on the surface of a growing fibre can act as a nucleation site for a new rod. An implication of Morse and Donnay's work is that the nucleation rate of rods is constant throughout the spherulitic growth process.

The results of the Arrhenius type plots presented in Figure 5 show that the measured activation energies of the crystallization process depend to a great extent on the nucleation treatment. The activation energy is reduced considerably by an increased nucleation time and phase separation, whereas the addition of TiO_2 affects the activation energy to a lesser degree.

If V_V in Equation 5, which includes the temperature dependence of the nucleation and growth process, is taken to be 0.5, the plots of $\ln t^{(0.5)}$ versus $1/T$ are identical to those shown in Figure 5. The exponential term in Equation 5 suggests that what is normally measured as the temperature dependence of the glass crystallization process is a combination of the acti-

vation energy for nucleation and the activation energy for growth, where the measured value depends not only on the individual activation energies, but also on the morphology of the growing phase. It should be pointed out that the growth morphology must remain constant with temperature in order for the activation energy to have any real meaning. Since the average activation energy for the growth of $\text{Li}_2\text{Si}_2\text{O}_5$ crystals has been shown to be approximately 56 Kcal/mole,¹⁻² and since it was shown in this experiment that n at the early stages of growth does not vary appreciably with nucleation treatment, then the effect of TiO_2 , phase separation in the 25 mole % glass, or an increased nucleation time seems to be one of decreasing the activation energy for nucleation.

Looking at the crystallization process as a whole, it is theorized that structural rearrangements tending toward the coordination of stable nuclei occur during the nucleation heat treatment. During the growth period, the embryo grow into stable nuclei of $\text{Li}_2\text{Si}_2\text{O}_5$, but the spherulitic type nucleation and growth of rods begins only after these nuclei have grown to a critical size. Evidence of this fact is given by the Guinier-DeWolff data and the plots of Equation 3, the slopes of which yield a physically meaningful value for nucleation and growth only when plotted from the point $V_V = 0$. The narrow size distribution of crystals seen in the micrographs (~3%) indicates that the free energy of all the nucleation sites formed during the nucleation treatment were approximately equal, and that all the crystal nuclei formed at nearly the same time. Further investigations of the initial stages of nucleation and growth are to be reported in a later paper.²²

Summary and Conclusions

The JMA equation and petrographic sections were employed to show a spherulitic crystallization mode of $\text{Li}_2\text{Si}_2\text{O}_5$ from glasses in the $\text{Li}_2\text{O}-\text{SiO}_2$

system. A modified version of this same equation was used to show that the measured activation energy was a combination of the activation energies of both nucleation and growth, and a factor determined by the dimensionality of crystal growth. The measured activation energies varied with both composition and heat treatment. Since growth morphology was rod-like in all cases and the activation energy of crystal growth is constant at 56 Kcal/mole, it can be concluded that the activation energy for nucleation of rods varies for the different samples. It is also expected that the kinetics of the rearrangement process occurring during the nucleation treatment are likewise affected by the different conditions. This could be manifested in the variation in incubation period between the series of samples.

The overall result of this study was to show that various nucleation treatments such as phase separation, the addition of a nucleating agent, and heat treatment can drastically change both the rate of crystallization at a given temperature and the temperature dependence of the process. Further work is needed to determine the exact mechanism of nucleation in each of these cases.

ACKNOWLEDGMENTS

The authors would like to thank Dr. R. T. DeHoff of the University of Florida for his help in analyzing the data, and to thank Mr. E. J. Jenkins for his help in obtaining the electron micrographs used in this study.

REFERENCES

1. R.J. Jaccodine, "Study of Devitrification of Lithium Glass," J. Am. Ceram. Soc., 44 [10] 472-75 (1961).
2. J.G. Morley, "Crystallization Kinetics in Some Silicate Glasses. Part 2. A Study of Crystallization Kinetics in the System $\text{Li}_2\text{O-SiO}_2$," Glass Technology, 6 [3] 77-89 (1965).
3. G.E. Rindone, "Further Studies of the Crystallization of a Lithium Silicate Glass," J. Am. Ceram. Soc., 45 [1] 7-12 (1962).
4. J. Matsuda and E. Suito, "Studies of the Crystallization of Lithium Silicate Glass," Kogyo Kagaku Zasshi, 67 [6] 884-86 (1964).
5. S.M. Ohlberg and D.W. Strickler, "Determination of Percent Crystallinity of Partly Devitrified Glass by X-ray Diffraction," J. Am. Ceram. Soc., 45 [4] 170-71 (1962).
6. E.A. Porai-Koshits and V.I. Aver'yanov, "Electron Microscopic Investigation of Heterogeneous Structure and Initial Crystallization Stages of Glasses in the System $\text{Li}_2\text{O-SiO}_2$," The Structure of Glasses, 5, 63-81; translated by Consultants Bureau Inc., New York, 1965.
7. W. Vogel and K. Gerth, "Catalyzed Crystallization in Glass," Symposium on Nucleation and Crystallization in Glasses and Melts, pp. 11-22, American Ceramic Society, Columbus, Ohio, 1962.
8. S.M. Ohlberg, H.R. Golob, and D.W. Strickler, "Crystal Nucleation by Glass in Glass Separation," ibid, pp. 55-62.
9. R.H. Munch and E.D. Pierron, "Practical Method of Powder Sample Preparation for X-ray Diffraction," Norelco Reporter, X [2] 75-76 (1963).
10. D. Turnbull and M.H. Cohen, Modern Aspects of the Vitreous State, p. 45; Butterworths Scientific Publications, London, 1963.
11. W.B. Hillig and D. Turnbull, "Theory of Crystal Growth in Undercooled Pure Liquids," J. Chem. Phys. 24, 914 (1956).
12. J. Frenkel, Kinetic Theory of Liquids; pp. 415 and 424, Clarendon Press, Oxford, 1946.
13. W.A. Johnson and R.F. Mehl, "Reaction Kinetics in Processes of Nucleation and Growth," Trans. AIME, 135, 416 (1939).
14. M. Avrami, "Kinetics of Phase Change I. General Theory," J. Chem. Phys., 7, 1103 (1939).
15. J.E. Burke and D. Turnbull, "Recrystallization and Grain Growth," Prog. Met. Phys., 3, 220 (1952).
16. R.T. DeHoff; private communication.

17. W.H. Sas and P.M. DeWolff, "Intensity Corrections for the Guinier Camera," Acta. Cryst., 21, 826-827 (1966).
18. D.L. Kinser and L.L. Hench, "Effect of Metastable Precipitate on the Electrical Properties of a $\text{Li}_2\text{O-SiO}_2$ Glass," to be published.
19. M.A. Matveev and V.V. Velya, "A Study of the Crystallization of Lithium Glasses in the System $\text{Li}_2\text{O-SiO}_2$," Glass and Ceramics, XVI, 543-9 (1960); Russian original, Steklo i Keramika, January-April (1959).
20. A.I. Korelova, M.G. Degen, and O.S. Alekseeva, "Microstructure of the Two-Component Lithium Silicate Glasses at Various Crystallization Stages," The Structure of Glass-Catalyzed Crystallization of Glass, 3, 65-68, translated by Consultants Bureau Inc., New York (1964).
21. H.W. Morse and J.D. H. Donnay, "Optics and Structure of Three Dimensional Spherulites," Am. Mineralogist, 21, [7] 391-426 (1936).
22. L.L. Hench, S.W. Freiman, and D.L. Kinser, "The Early Stages of Crystallization of Glasses," to be published.

TABLE I

PREVIOUS STUDIES OF CRYSTALLIZATION IN $\text{Li}_2\text{O-SiO}_2$ SYSTEMS

Author	Method	Volume Percent	Composition (Mole % Li_2O)	Nucleation	Activation Energy ^a (Kcal/mole)
G. E. Rindone	X-ray	20.	20.	none	120
		.001% Pt	20.	.001% Pt	95
		.005% Pt	20.	.005% Pt	50
		>.005% Pt	20.	>.005% Pt	60
J. G. Morley	High Temperature, Optical, Crystal Growth	33.3	26.15	10 min at 400°C; Surface (-3 '0 mesh samples)	49
			27.3	none	54 ^c
			28.3	none	52 ^c
R. J. Jaccodine	Optical, Crystal Growth	30.	30.	none	49

^aAverage activation energy based on the values obtained by Morley and Jaccodine is 56.

^bMethod of Ohlberg and Strickler.⁵

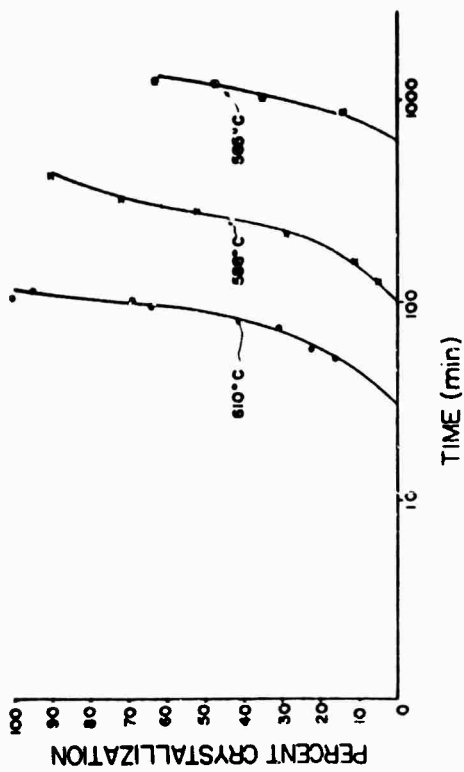
^cCalculated by the authors from Morley's data.

TABLE II
 EXPERIMENTAL CONDITIONS AND MEASURED ACTIVATION ENERGIES

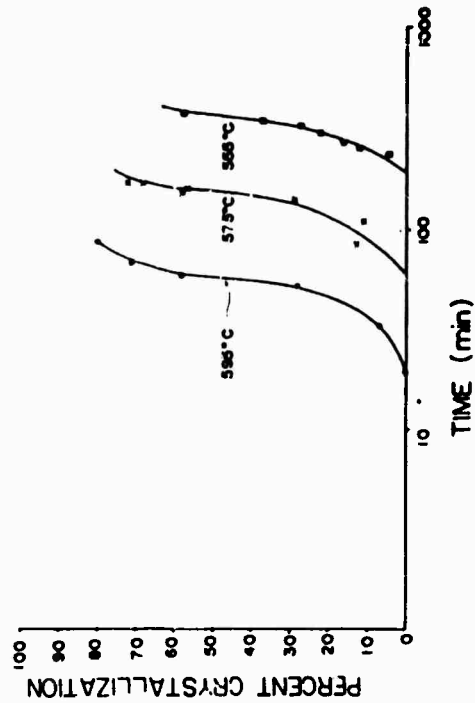
Sample Series	Composition (mole %)		Melting Temp. (°C)	Nucleation Treatment at 475°C (hr)	Activation Energy (Kcal/mole)
	SiO ₂	Li ₂ O TiO ₂			
A	66.7	33.3 0.0	1350	3	92
B	64.2	32.1 3.7	1350	3	77
C	66.7	33.3 0.0	1350	24	52
D	75.0	25.0 0.0	1415	3	49

TABLE III
 EXPERIMENTAL SLOPES OF THE MODIFIED FORM OF THE
 JMA EQUATION (EQUATION 3)

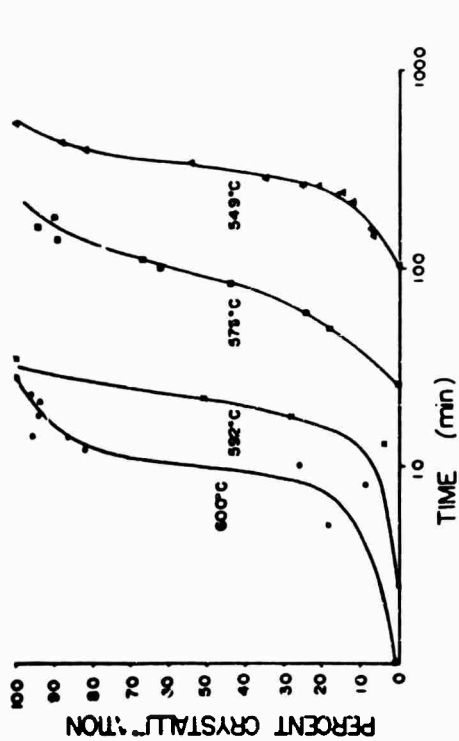
Sample Series	Growth Temperature (°C)	Slopes of Equation 3 (n + 1)	n
A	600	2.3	1.3
	575	1.4	0.4
	549	1.4	0.4
B	610	1.7	0.7
	588	1.5	0.5
	565	1.7	0.7
C	595	2.0	1.0
	575	1.9	0.9
	555	1.6	0.6
D	595	1.8	0.8
	575	1.3	0.3
	555	1.2	0.2



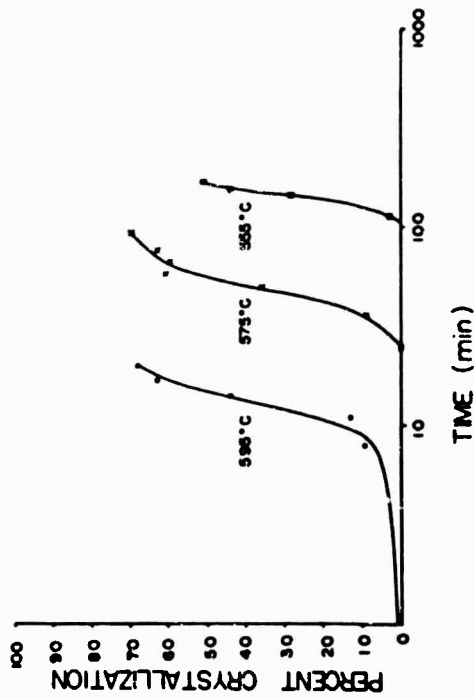
(B) $\text{SiO}_2 + 33.3 \text{ mole } \% \text{Li}_2\text{O} + 3.7 \text{ mole } \% \text{TiO}_2$,
3 hr at 475°C



(D) $\text{SiO}_2 + 25 \text{ mole } \% \text{Li}_2\text{O}$, 3 hr at 475°C



(A) $\text{SiO}_2 + 33.3 \text{ mole } \% \text{Li}_2\text{O}$, 3 hr at 475°C



(C) $\text{SiO}_2 + 33.3 \text{ mole } \% \text{Li}_2\text{O}$, 24 hr at 475°C

Figure 1 Crystallization of $\text{Li}_2\text{Si}_2\text{O}_5$ from $\text{Li}_2\text{O-SiO}_2$ glass.



Fig. 2 Electron micrograph of a spherulite on a fracture surface from series A (X2500).

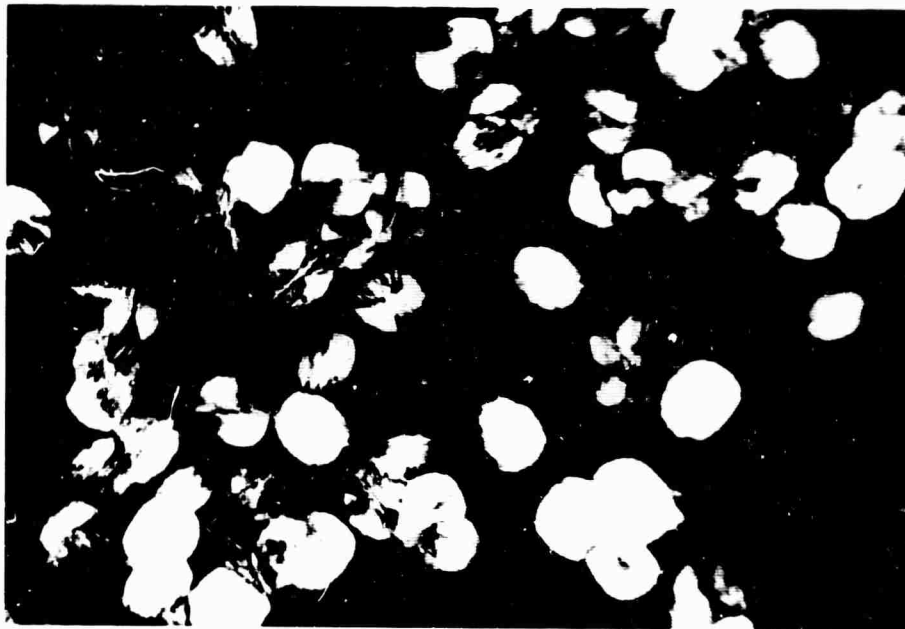


Fig. 3 Thin section of sample from series B, $V_V = 0.41$, crossed nicols (X125).

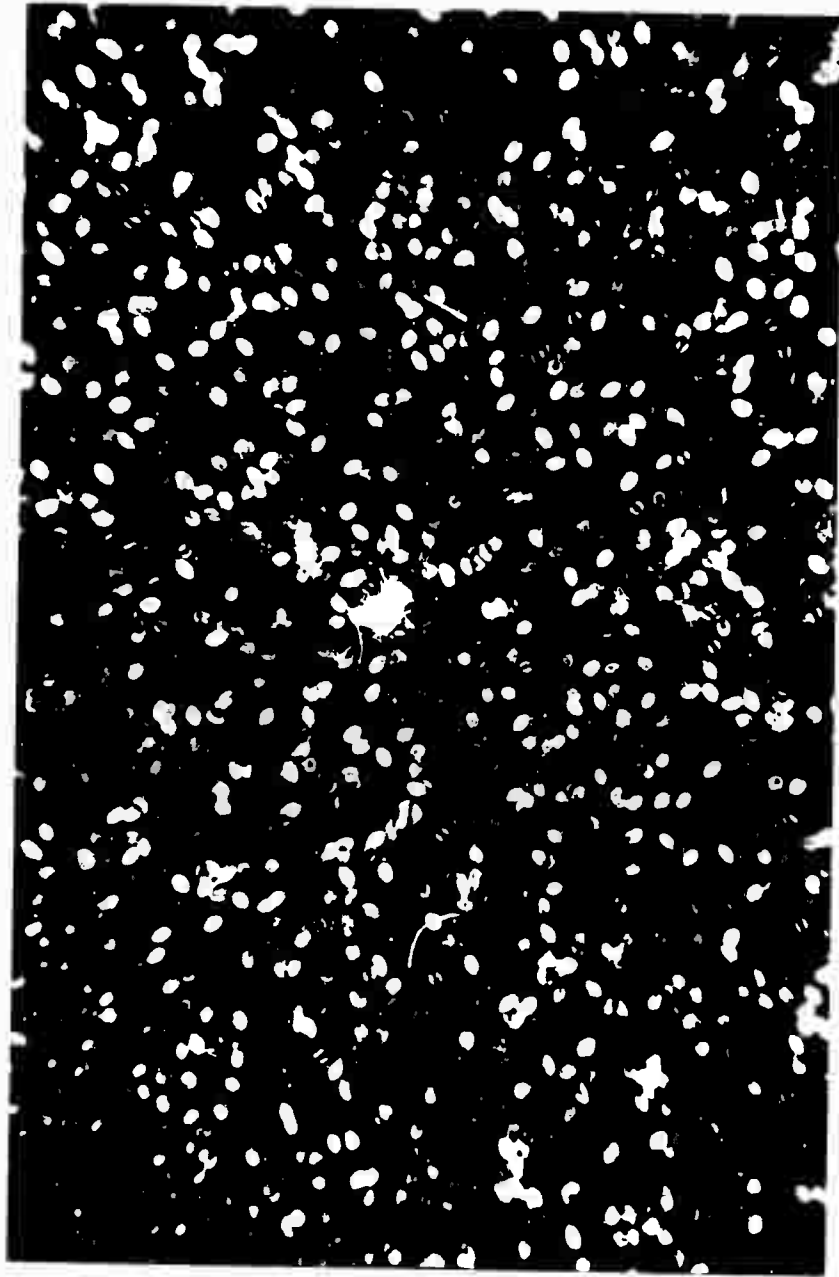


Fig. 4 Thin section of sample from series D, $V_V = 0.42$,
crossed nicols (X125).

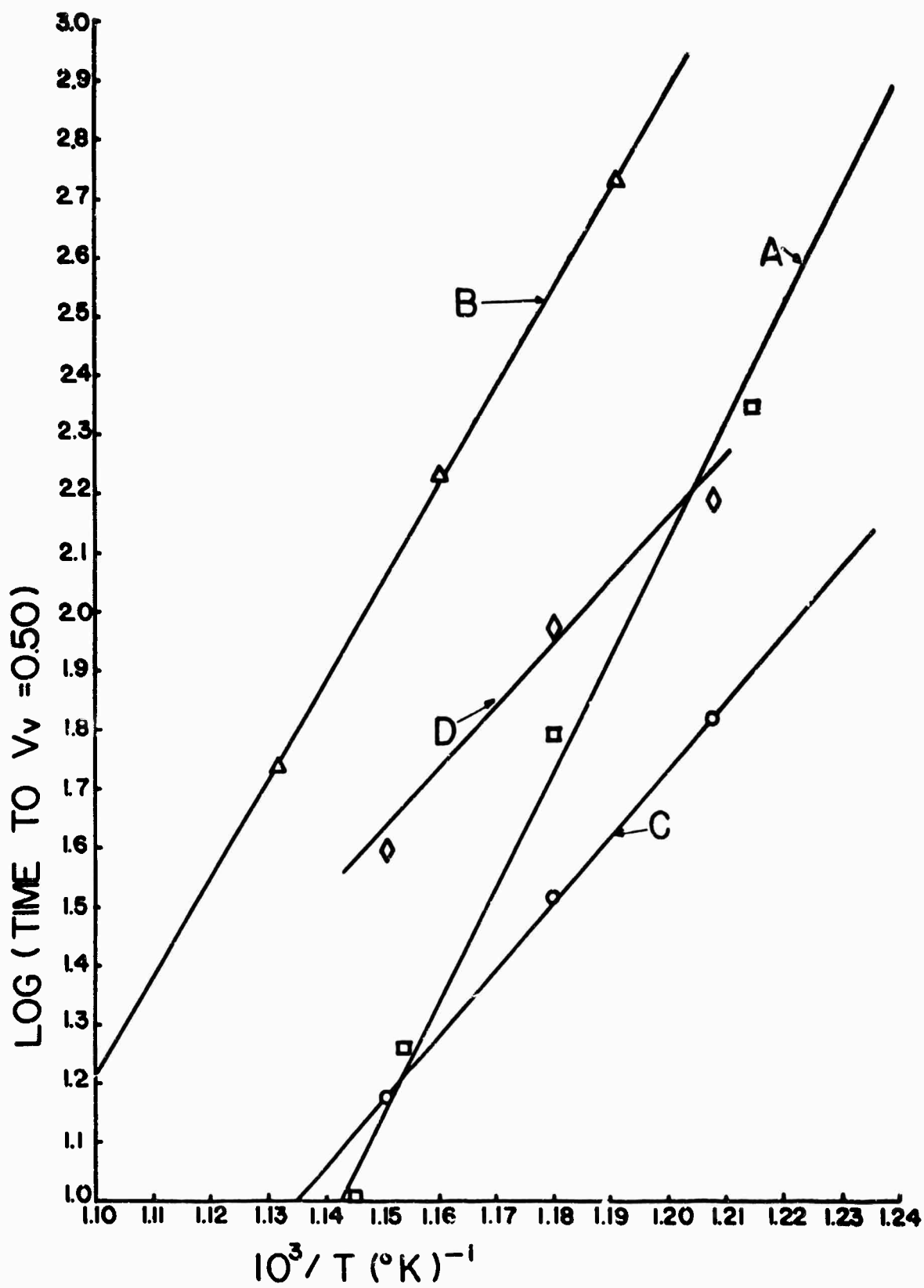


Fig. 5 Temperature dependence of crystallization rate. Crystallization assumed to begin at $V_v = 0$.

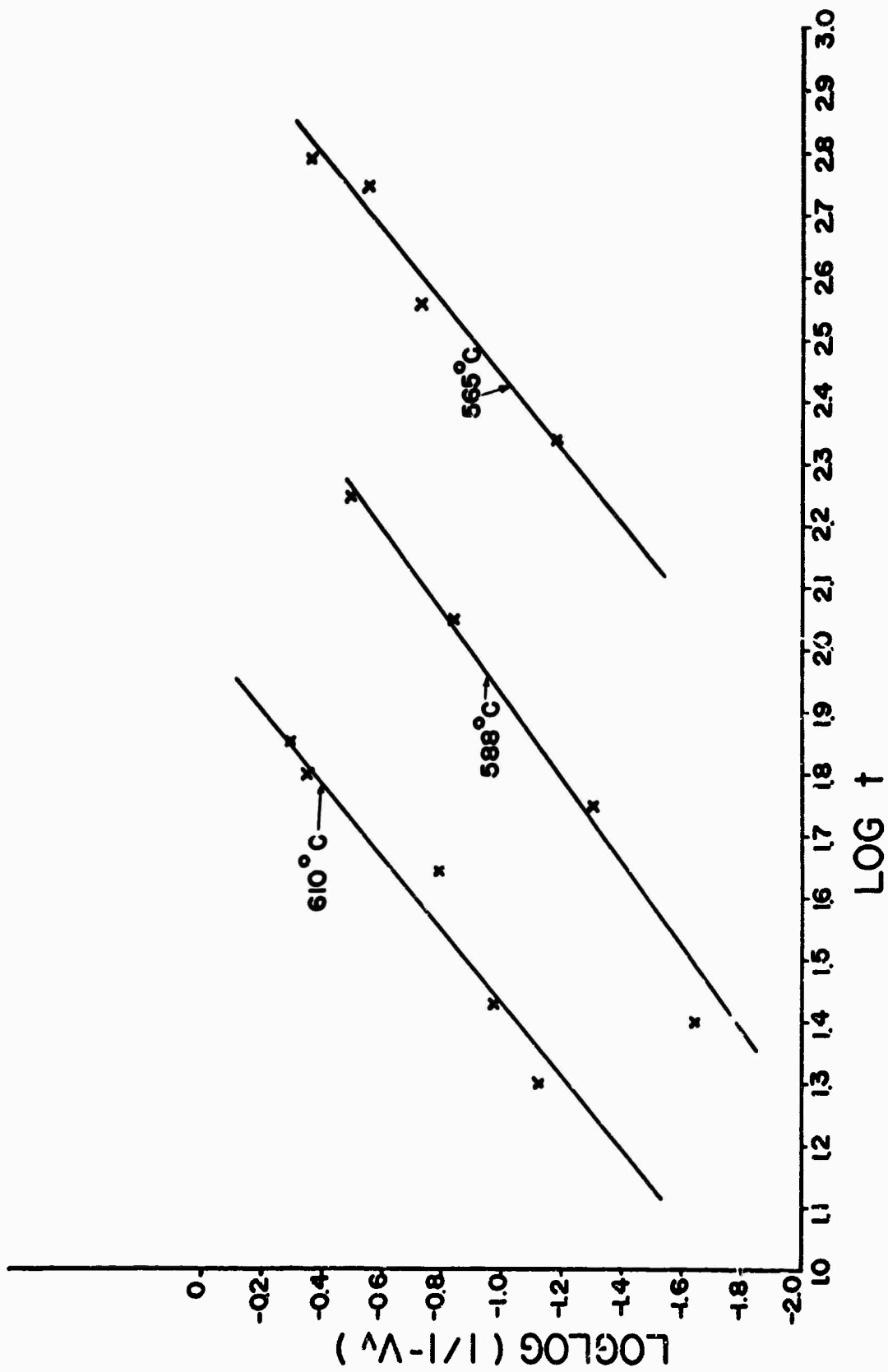


Fig. 6 Determination of the morphology of the crystallization process for series B using Equation 3.

B. EFFECT OF A METASTABLE PRECIPITATE ON THE ELECTRICAL PROPERTIES OF A $\text{Li}_2\text{O-SiO}_2$ GLASS

Introduction

It has been recognized for many years that thermal treatments in the annealing-transformation range significantly alter the dc conductivity of glasses.¹⁻² The internal friction work of Day and Rindone³ on lithia-silica glasses has shown that relaxation loss peaks appear during the process of thermal treatments in the same temperature range. Owen's work⁴ with Cabal glasses has shown that similar thermal treatments produce changes in ac dielectric adsorption spectra.

Charles⁵ has examined the electrical properties and structural differences in lithia-silica glasses resulting from different quenching rates. His analysis indicated that the variation of the dielectric loss behavior with quenching rates can be rationalized in terms of the morphology of phase separation in the glasses, and the Maxwell-Wagner-Sillars (MWS) heterogeneous dielectric model.^{6,8}

It was the objective of the present work to determine the changes in structure and electrical properties of a 17.5 weight % $\text{Li}_2\text{O-SiO}_2$ glass during an isothermal heat treatment in the annealing-transformation range (500°C). The present results indicate that the changes observed are due to the appearance of a metastable crystalline lithium metasilicate precipitate.

Experimental Procedure

Specimen Preparation

The glass used in these experiments was prepared from 99.9% silica (5 MinUSil^{*}), and 99.3% lithium carbonate,^{**} blended in a jar mill and melted

* Pennsylvania Glass Sand Co.

** Foote Mineral Company

24 hours in a covered platinum crucible at 1350°C. Specimens 1.79 cm in diameter and approximately 0.5 cm thick were cast in a steel mold and annealed 1 hour at 300°C.

Electrical Measurements

The surfaces of the electrical specimens were ground to achieve parallelism and double guard ring gold electrodes were vapor deposited on the ground surfaces. Measurements were carried out in a specially designed sample holder,⁹ which allowed the specimen to be heated under a vacuum of less than 1 micron.

The dc values were measured utilizing a Beckman picoammeter and a standard dc supply with guarded leads. Ac properties were measured using a bridge type apparatus shown schematically in Figure 1. This equipment allowed measurements of conductance and capacitance over the frequency range of 100 Hz to 1 MHz with three significant figures.

Heat treatments were carried out in an air atmosphere tube furnace with temperature control of $\pm 1^\circ\text{C}$. The gold electrodes were removed during heat treatments to prevent diffusion of gold into the glass.

X-ray Studies

X-ray analyses were carried out on specimens prepared in the same manner as the electrical specimens. Samples were heat treated, then ground to ~200 mesh and examined in a vacuum Guinier-DeWolff¹⁰ camera using copper K α radiation. This technique allowed detection and identification of as little as 0.1 weight percent crystal.¹¹

Electron Microscopy

Carbon replicas of platinum preshadowed etched fracture surfaces were examined in a Philips EM 200 electron microscope.

Results

Electrical Measurements

The results of the ac measurements are presented in the form of the ac loss angle ($\tan \delta_{ac}$) as a function of frequency and temperature. The $\tan \delta_{ac}$ values were calculated from the measured values of capacitance and conductance following the method of Charles.⁵ The tangent of the loss angle is shown as a function of log frequency for the different heat treatments and measuring temperatures in Figures 2-6.

It can be noted from Figure 2 that the as cast glass is free of loss peaks, but after a $5 \pm 1/2$ hour heat treatment (Figure 3) at 500°C , large peaks have appeared. Further heat treatments at the same temperature for times up to 50 hours (Figures 4-6) cause the magnitude of $\tan \delta_{ac}$ to decrease and the position of the maxima (f_{max}) to shift to higher frequencies. The temperature dependence of the frequency maxima in the $\tan \delta_{ac}$ curves is shown in Figure 7.

The logarithm of the dc conductivity obtained is shown as a function of reciprocal temperature in Figure 8. The dc conductivity of the glass generally decreases with heat treatment while the activation energy is unchanged within the limits of the experimental error.

Table I shows a comparison of the present results and the work of several other investigators in glasses of approximately the same composition. The dc activation energies shown all agree within the probable experimental errors. The activation energy for the ac relaxation agree well with those of Charles⁵ on the same glasses.

Figure 9 shows the magnitude of $\tan \delta_{ac}$ and the dc conductivity as a function of heat treatment time. The initial increase in $\tan \delta_{ac}$ is not accompanied by a change in the dc conductivity.

X-ray

The lattice spacings from the Guinier-DeWolff camera films are shown in Table II. The actual patterns are not presented because the lines of interest are very weak even after 50-hour exposures and photographic reproduction is difficult. Examination by the above technique showed no crystalline lines for the as cast glass or after a 20-hour heat treatment, and consequently, they were omitted from the table. The two patterns showed only a broad diffuse peak characteristic of the glassy state. The disilicate standard is slightly off stoichiometry and as a result showed three weak lines from the metasilicate. The sample which has been heat treated for 5 hours shows seven lines, three of which correspond to the stronger metasilicate lines. The other four lines are weaker and are, at present, not conclusively identified. It appears that the unidentified lines correspond to a transition phase of lower symmetry than the orthorhombic metasilicate. Indexing is difficult, if not impossible, because of the small number of lines observed. This transition type phase of lower symmetry has been observed in the pre-precipitation stages of age hardening metallic alloys.¹² The four strongest disilicate lines are observed for the 50-hour specimens.

Electron Microscopy

The EM results are summarized in Figure 10. These micrographs show a large dispersed droplike phase in the as cast glass (A). After a 5-hour heat treatment at 500°C, a fine precipitate appears in the matrix surrounding these drops (B). With further heat treatment the structure seems to become more homogeneous while the primary and secondary precipitates begin to disappear (C).

Discussion

Initial Structure

The electron micrographs of the as cast glass shows silica rich drops in

a lithia rich matrix. This structure can be rationalized if the metastable liquid-liquid immiscibility, which is well known in this system,¹³⁻¹⁴ is extended into the disilicate-metasilicate field as shown in Figure 11. Cooling the liquid 17.5 weight % composition results in a silica rich glassy phase and a glassy phase with a composition richer in lithia than the disilicate. In the $\text{Li}_2\text{O-SiO}_2$ glass system the dc conductivity of the glass increases with increasing lithia content,¹⁵ thus the lithia rich matrix of the as cast glass described above has higher conductivity than the dispersed silica rich phase. This morphology gives a high dc conductivity because the lithia rich phase is connected.

The above structure does not give rise to dielectric loss peaks because the MWS model requires that the dispersed phase be the highly conducting phase.

Appearance of Loss Peaks

The MWS heterogeneous dielectric theory predicts that large losses will occur when a highly conducting phase is dispersed in a matrix of much lower conductivity. Electron micrographs of the glass after a 5-hour heat treatment show the appearance of a second dispersed phase. The x-ray results indicate that this phase, which appears concurrently with the loss peaks, is crystalline lithium metasilicate.

The structure when the loss peaks are large (5-hour heat treatment) consists of highly conductive metasilicate crystals dispersed in a silica rich matrix. This structure has the necessary properties to give rise to loss peaks as predicted by the MWS heterogeneous dielectric theory.

Disappearance of Loss Peaks

The EM results show that the metasilicate dispersed phase has begun to disappear after 10 hours at 500°C . During this thermal treatment the conditions for the MWS heterogeneous losses are being eliminated so the magnitude of the

loss peaks is reduced. In order to explain the above behavior, it is helpful to construct a free energy composition diagram corresponding to the heat treatment temperature (500°C). This diagram (Figure 12) was constructed from free energy values for the stoichiometric compounds obtained by assuming a linear relationship to the corresponding soda-silicate compounds which are available in the literature. The free energy of formation of lithium metasilicate, sodium silicate, and the sodium metasilicate was obtained from Richardson, Jeffes and Withers.¹⁶ The direction of change of free energy for the nonstoichiometric compounds was inferred from first principles,¹⁷ while the relative values for the liquids were inferred from the phase diagrams.

Considering the as cast microscopic heterogeneous mixture described above at the heat treatment temperature, the free energy (Figure 12) of the matrix G_2 can be reduced by separation into metasilicate crystals G_5 and a silica rich glass G_4 . Behavior of this type has also been postulated by Roy.¹⁸ This reduces the free energy of the matrix from G_2 to G_7 and the free energy of the overall glass from G_3 to G_6 . As the thermal treatment proceeds, the metasilicate crystals G_5 react with the silica rich drops G_1 to form the equilibrium disilicate G_8 . This process further reduces the overall free energy from G_6 to G_9 . If the process is allowed sufficient time to reach equilibrium, the free energy of the system is further reduced by the crystallization of the silica glass to quartz, thus attaining the equilibrium free energy G_{10} . Morely¹⁹ has shown evidence for this last step in the crystallization of quartz in these glasses.

The free-energy-composition diagram allows one to follow the "state" of the glass through a series of non-equilibrium states as described above. The appearance of the highly conducting lithium metasilicate in the silica rich matrix gives rise to the large dielectric losses which appear concurrently with the lithium metasilicate crystals. The subsequent reduction in the height

of the loss peaks is due to the reaction of the highly conductive metasilicate phase to form the disilicate phase. The shift of the $\tan \delta_c$ -frequency maxima towards higher frequencies with heat treatment is probably due to changes in conductivity of the crystalline lithium metasilicate precipitate. The variation results from compositional changes within the metasilicate solid solution range as well as from the compositional changes occurring in the glassy matrix.

Conclusions

On the basis of the x-ray and electron microscopy results, it can be concluded that the dielectric relaxation loss peaks occur due to the appearance of metastable lithium metasilicate crystals in the glass during a heat treatment of 5 hours at 500°C. At longer thermal treatments, the dielectric loss peaks decrease due to the resorption of the lithium metasilicate crystals. It seems quite likely that the appearance and subsequent resorption of a metastable crystalline phase is a precursor to the equilibrium crystallization in many other systems of this type.

REFERENCES

1. J.W. Rebbeck, M.J. Muiligan and J.B. Ferguson, "The Electrolysis of Soda-Lime Glass, Part II," J. Am. Ceram. Soc., 8 [6] 329-337 (1925).
2. J.T. Littleton and W.L. Wetmore, "The Electrical Conductivity of Glass in the Annealing Zone as a Function of Time and Temperature," J. Am. Ceram. Soc., 19 [9] 243-245 (1936).
3. D.E. Day and G.E. Rindone, "Internal Friction of Progressively Crystallized Glasses," J. Am. Ceram. Soc. 44 [4] 161-167 (1961).
4. A.E. Owen, "Properties of Glasses in the System $\text{CaO-B}_2\text{O}_3\text{-Al}_2\text{O}_3$, Part II Dielectric Properties in Relation to Structure," Phys. Chem. Glasses, 2 [5] 152-162 (1961).
5. R.J. Charles, "Some Structural and Electrical Properties of Lithium Silicate Glasses," J. Am. Ceram. Soc., 46 [5] 235-243 (1963).
6. J.C. Maxwell, Electricity and Magnetism, Vol. 1, Clarendon Press, London (1892) p. 328.
7. K.W. Wagner, "Explanation of the Dielectric Behavior on the Basis of the Maxwell Theory," Archiv fur Elektrotechnica, 2 371-387 (1914).
8. R.W. Sillars, "Properties of a Dielectric Containing Semiconducting Particles of Various Shapes," J. Inst. Elec. Engrs. (London), 86 378-394 (1937).
9. D.L. Kinser and L.L. Hench, "Apparatus for Glass Dielectric Measurements," to be published.
10. W.H. Sas and P.M. DeWolff, "Intensity Corrections for the Guinier Camera," Acta. Cryst., 21 826-827 (1966).
11. D.L. Kinser and L.L. Hench, "Quantitative Analysis of Small Crystalline Fractions," to be published.
12. K. Krishna Rao, H. Herman, and E. Parthe, "The Structure of a Metastable, Trigonal Transition Phase in Quenched Aluminum-29 at.% Zinc," Mater. Sci. Eng., 1 162-166 (1966).
13. W. Vogel and H.G. Byhan, "The Structure of Binary Lithium Silicate Glasses," Silikattechnik, 15 [7] 212-218 (1964).
14. R.J. Charles, "Metastable Liquid Immiscibility in Alkali Metal Oxide-Silica Systems," J. Am. Ceram. Soc., 49 [2] 55-62 (1966).
15. O.V. Mazurin, Structure of Glass, Academy of Sciences USSR Press (1964) pp 5-49; translated by Consultants Bureau, Inc., New York (1965).
16. F.D. Richardson, J. Jeffes, and G. Withers, "The Thermodynamics of Substances of Interest in Iron and Steel Making, Part II, Compounds Between Oxides," J. Iron and Steel Inst., 166 [11] 213-245 (1950).

17. L.S. Darken and D.W. Gurry, Physical Chemistry of Metals, McGraw-Hill, New York (1953) pp 326-341.
18. R. Roy, "Phase Equilibrium and the Crystallization of Glass," Symposium on Nucleation and Crystallization in Glasses and Melts, American Ceramic Society (1962)
19. J.G. Morley, "Crystallization Kinetics in Some Silicate Glasses, Part 2, A Study of Crystallization in the System $\text{Li}_2\text{O}-\text{SiO}_2$," Glass Technology, 6 [3] 77-89 (1965).
20. F.C. Kracek, "The Binary System $\text{Li}_2\text{O}-\text{SiO}_2$," J. Phys. Chem., 34 2641-2650 (1930).
21. S.B. Holmquist, "Conversion of Quartz to Tridymite," J. Am. Ceram. Soc., 44 [2] 82-86 (1961).

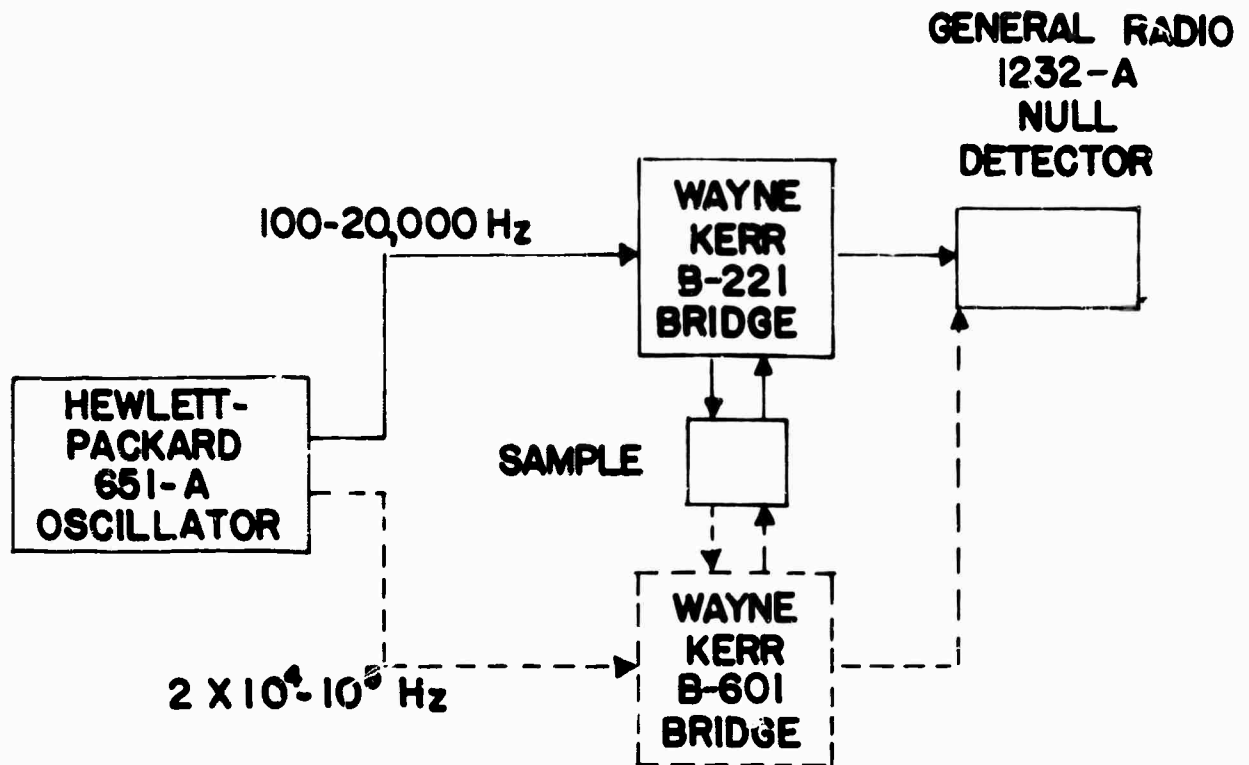
TABLE I
ACTIVATION ENERGIES

Composition (weight %)	Thermal Treatment (hr)	Dc Conductivity (Kcal/mole)	Ac Relaxation (Kcal/mole)	Source
17.5	0	15.7	- -	Present Investigation
17.5	5	15.7	14.7	Present Investigation
17.5	10	15.4	14.7	Present Investigation
17.5	20	- -	14.7	Present Investigation
17.5	50	16.9	- -	Present Investigation
17.5	"Normal"	19.6	14.6	Charles ⁵
17.5	Rapid Quench	14.6	14.6	Charles ⁵
19.5	Unknown	15.6	- -	Mazurin ¹⁵

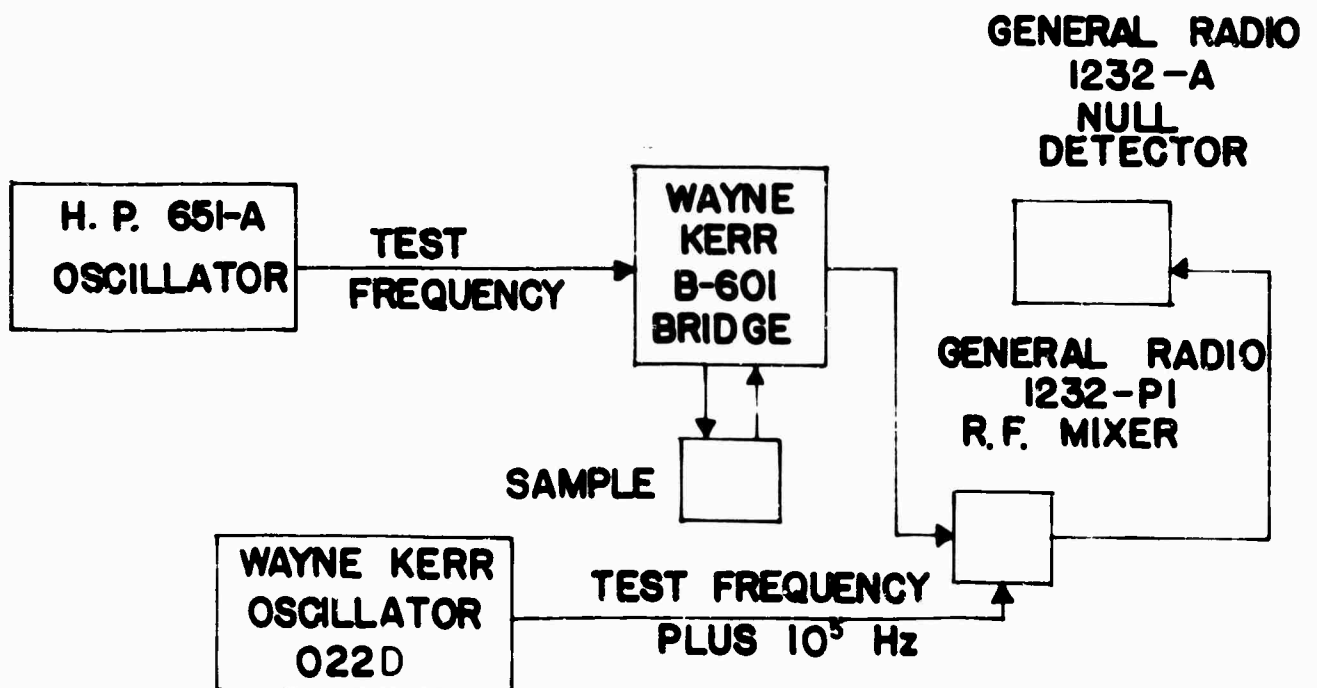
TABLE II

SUMMARY OF X-RAY LATTICE SPACINGS AND RELATIVE INTENSITIES

Standard $\text{Li}_2\text{O} \cdot 2\text{SiO}_2$		Standard $\text{Li}_2\text{O} \cdot \text{SiO}_2$		17.5 w/o Li_2O Heat Treated 5 hr at 500°C		17.5 w/o Li_2O Heat Treated 50 hr at 500°C	
d (Å)	Intensity	d (Å)	Intensity	d (Å)	Intensity	d (Å)	Intensity
7.4	2						
5.45	10					5.5	i
4.70	1 (M.S.)	4.70	10	4.70	1		
				4.35	1		
4.18	1			4.18	1		
3.75	10					3.75	1
3.65	10					3.65	1
3.58	10					3.58	1
3.30	1 (M.S.)	3.30	10	3.30	1		
2.95	1						
2.90	5			2.91	1		
				2.81	1		
2.70	1 (M.S.)	2.70	10	2.70	1		
2.39	5						
2.35	5	2.35	10				
2.27	2						
		2.08	2				



(a) Schematic diagram of the ac measuring apparatus. 100 Hz to 10^5 Hz.



(b) Schematic diagram of the ac measuring apparatus. 10^5 Hz to 10^6 Hz.

Fig. 1

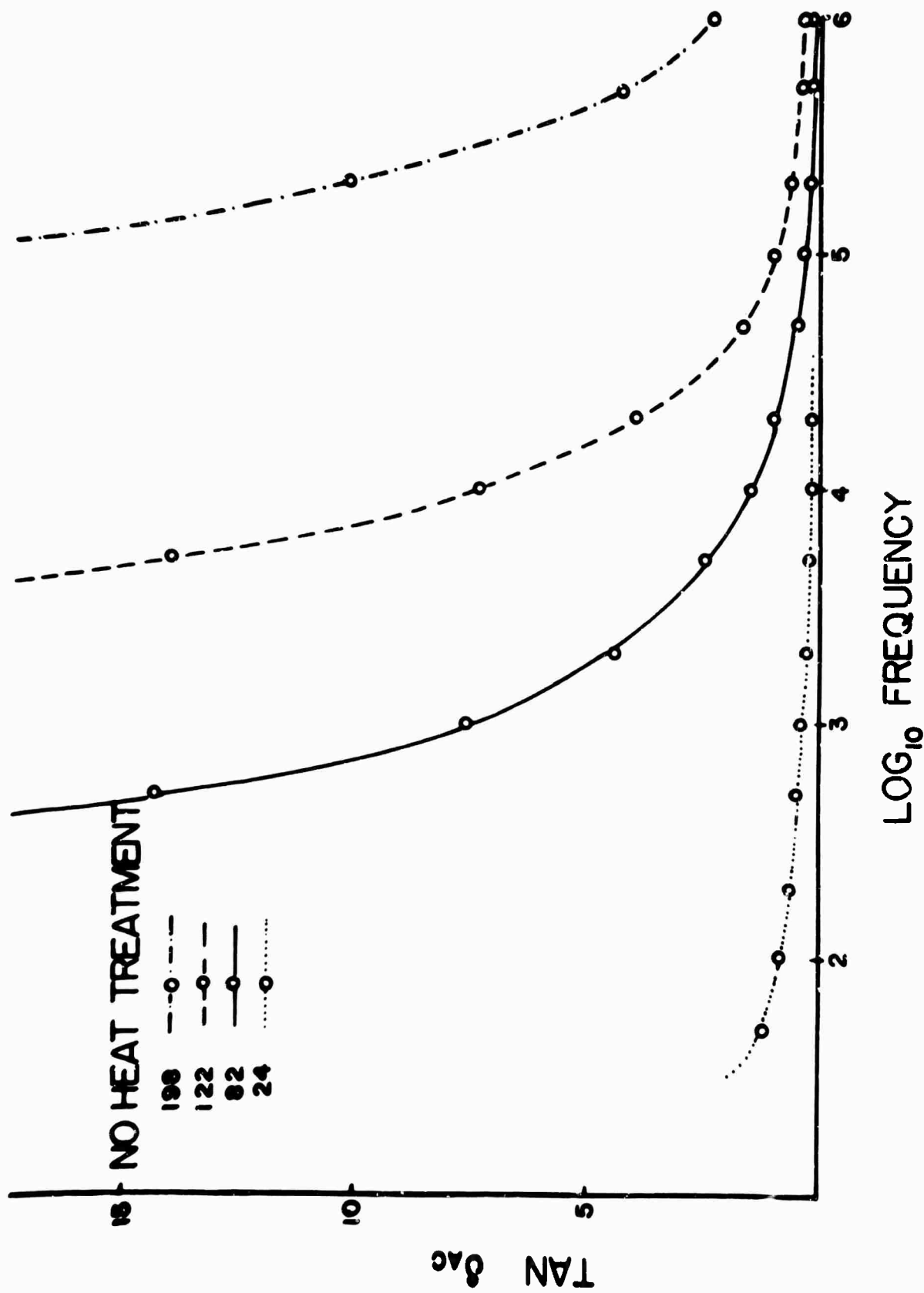


Fig. 2 Tan δ versus \log_{10} frequency for as cast 17.5 weight % $\text{Li}_2\text{O-SiO}_2$ glass.

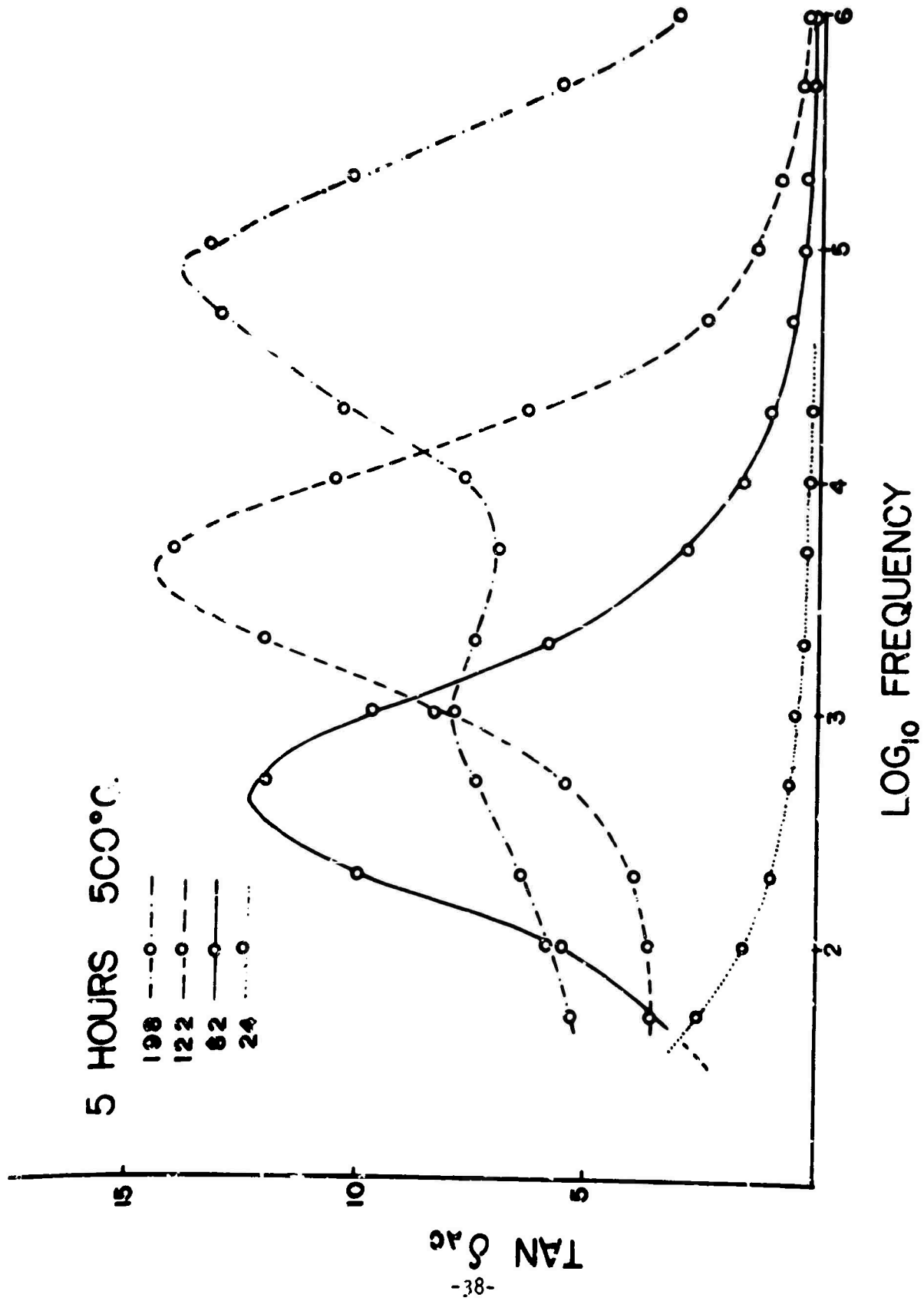


Fig. 3 Tan δ versus \log_{10} frequency for the 17.5 weight % $\text{Li}_2\text{O-SiO}_2$ glass heat treated 5 hours at 500°C.

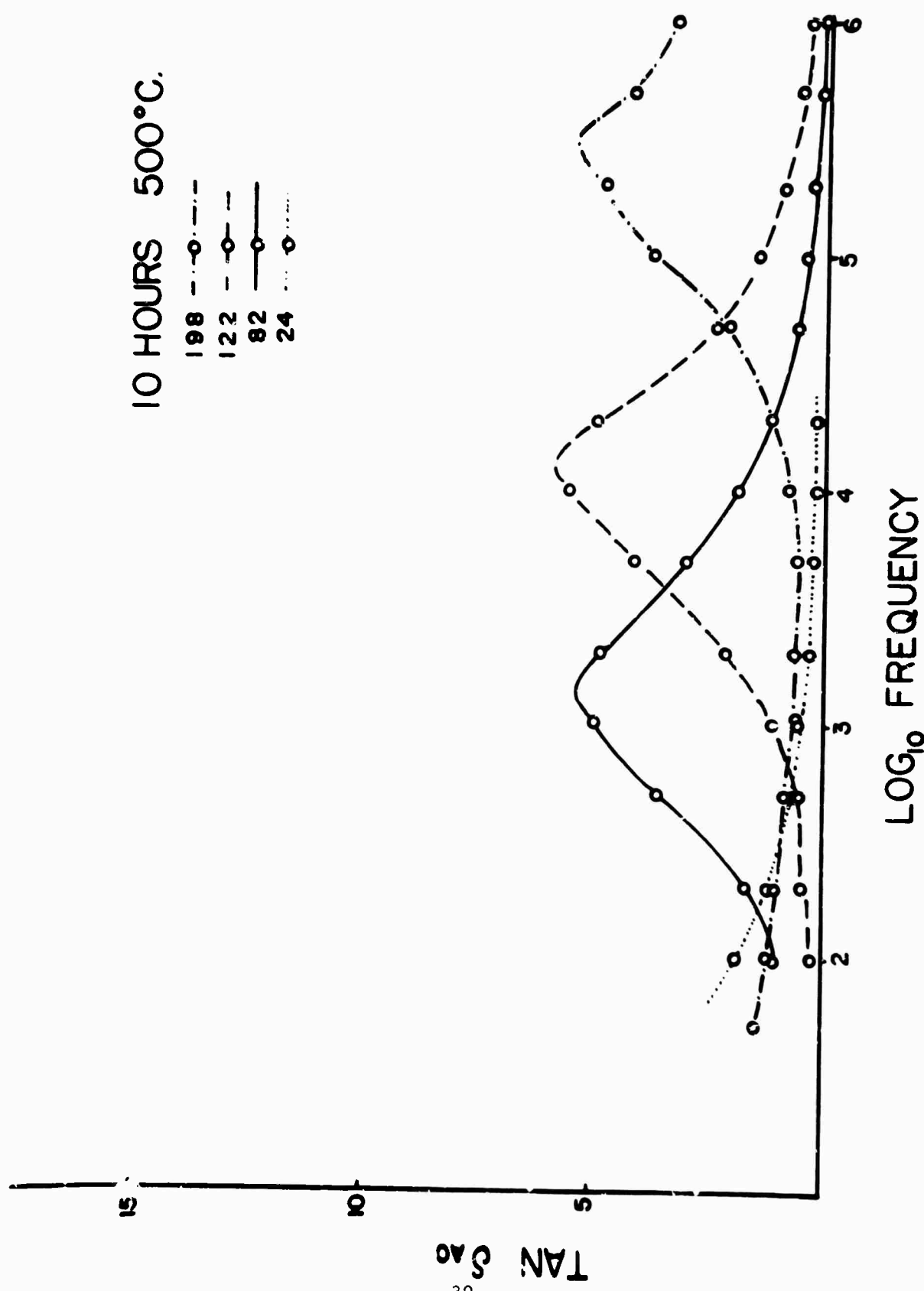


Fig. 4 Tan δ versus \log_{10} frequency for the 17.5 weight % $\text{Li}_2\text{O-SiO}_2$ glass heat treated 10 hours at 500°C.

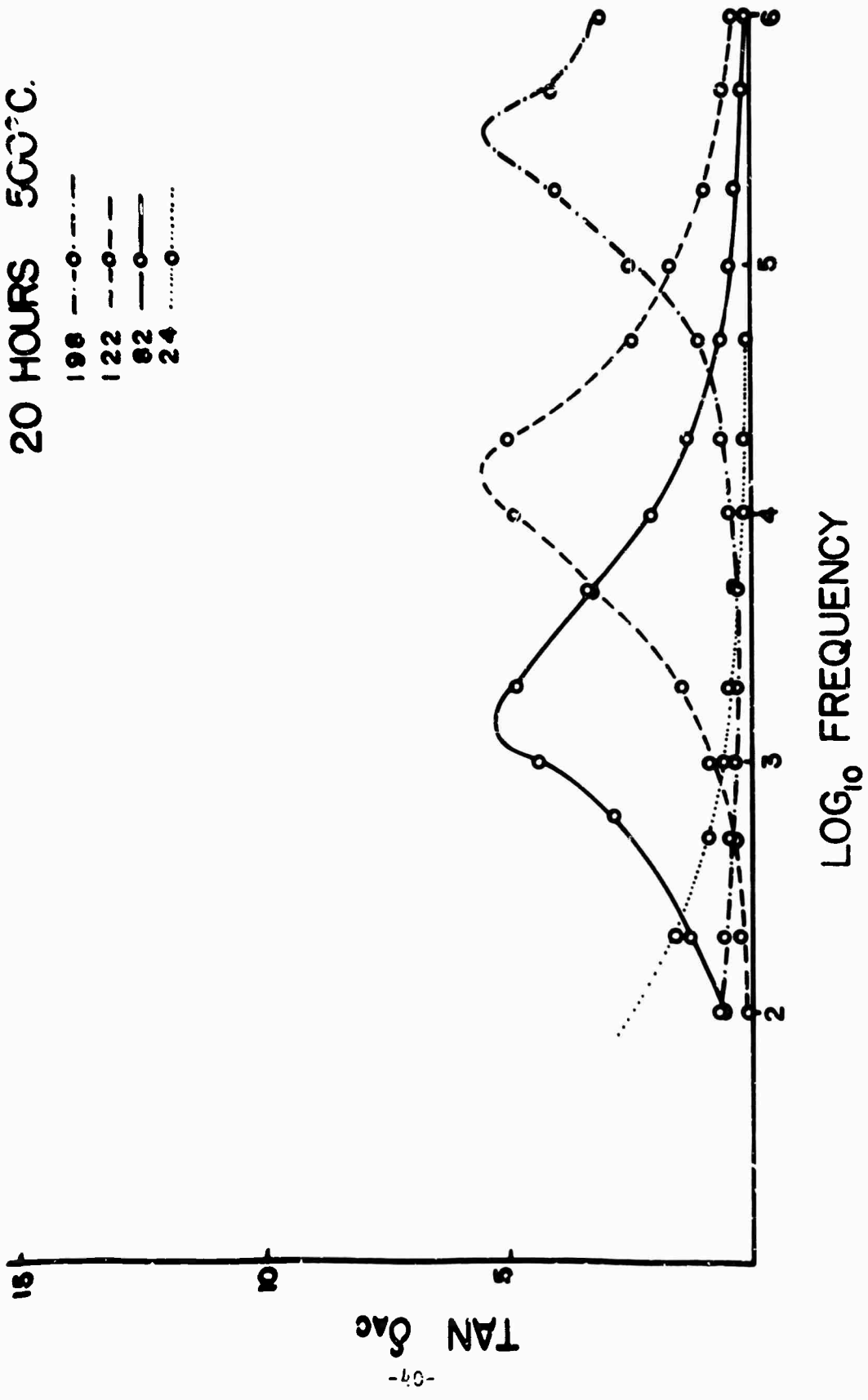


Fig. 5 Tan δ versus \log_{10} frequency for the 17.5 weight % $\text{Li}_2\text{O-SiO}_2$ glass heat treated 20 hours at 500°C

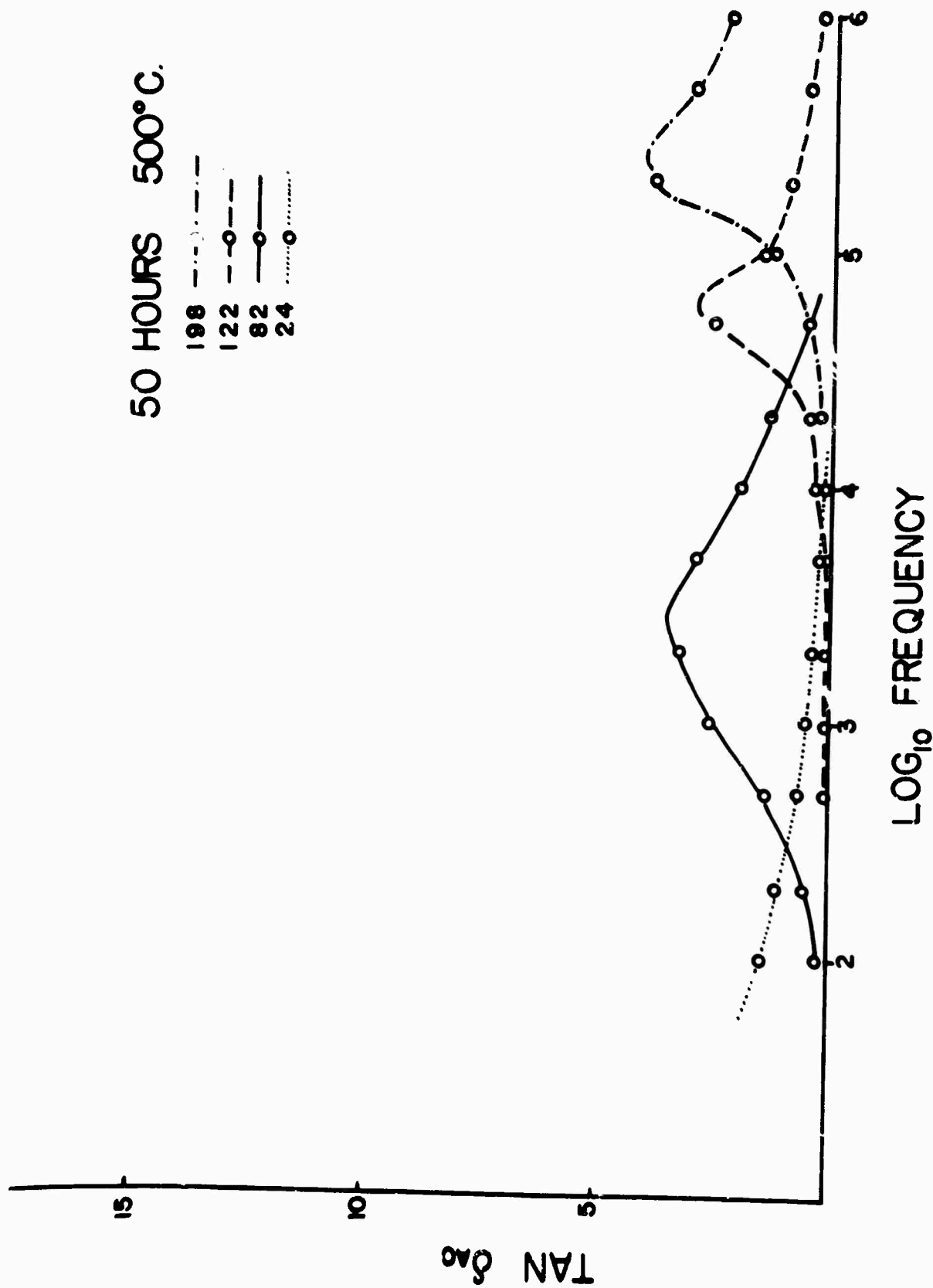


Fig. 6 $\tan \delta$ versus \log_{10} frequency for the 17.5 weight % $\text{Li}_2\text{O-SiO}_2$ glass heat treated 50 hours at 500°C.

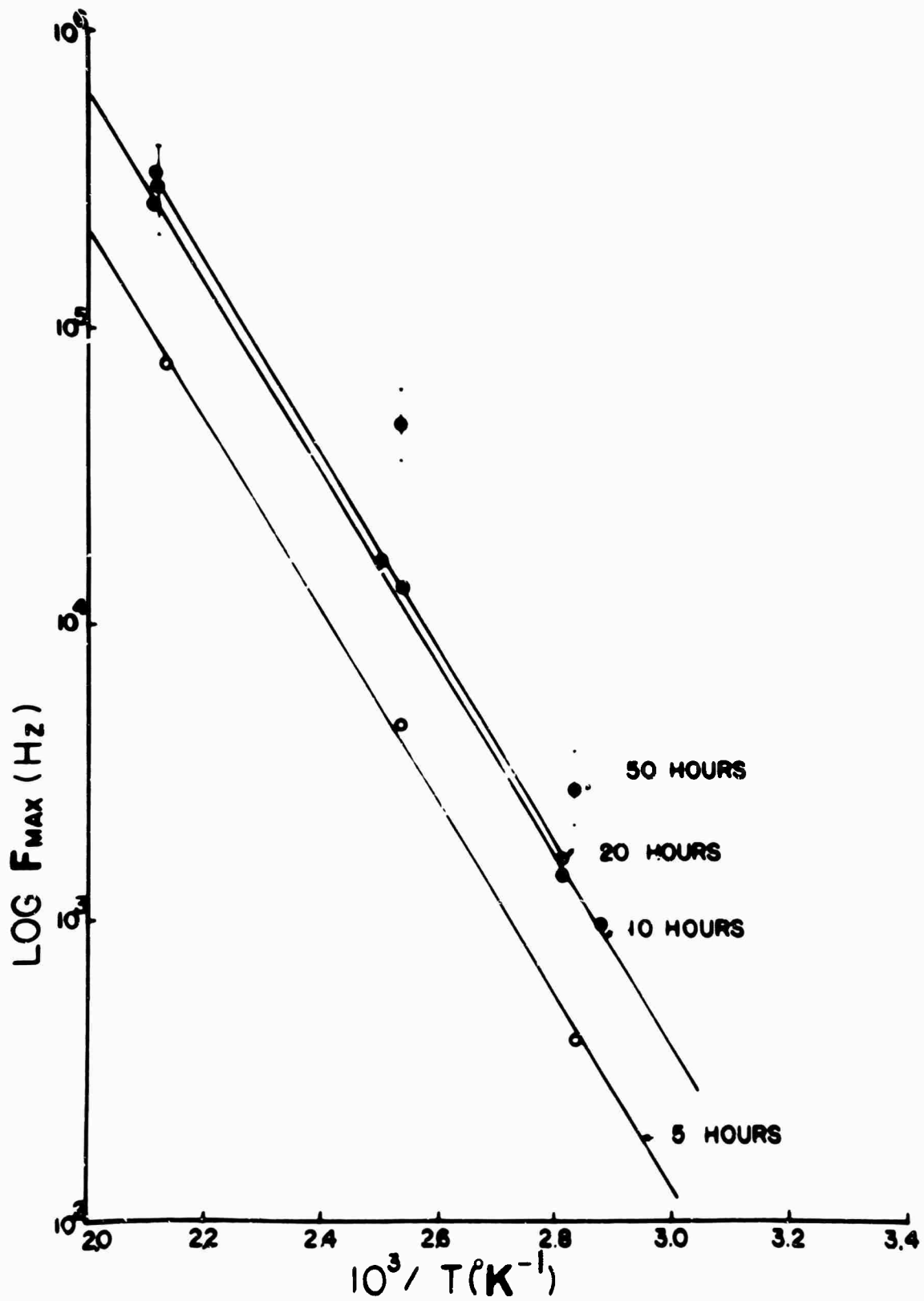


Fig. 7 Log of frequency maxima versus reciprocal temperature for various thermal treatments at 500°C.

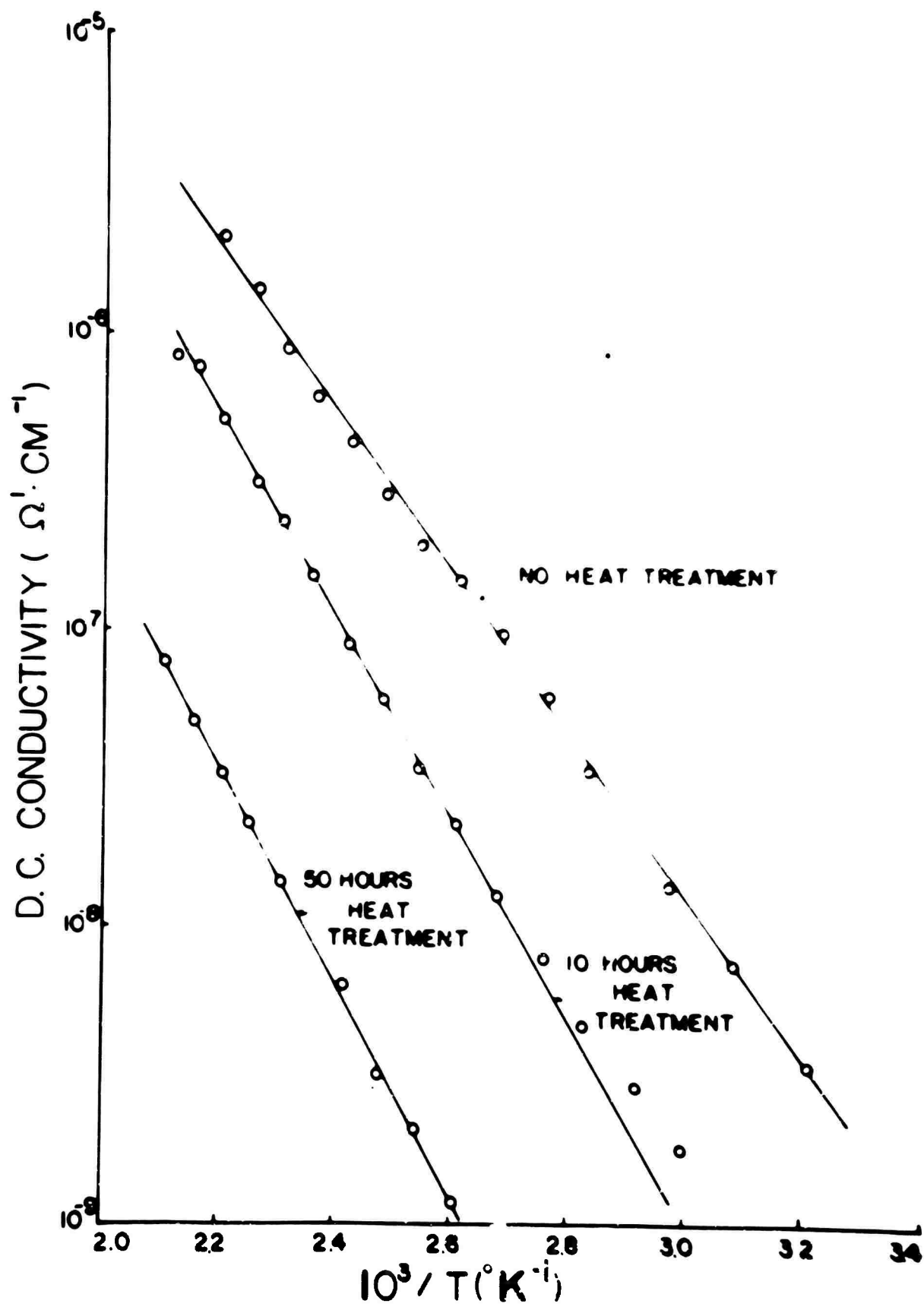


Fig. 8 Log of dc conductivity versus reciprocal temperature for various thermal treatments at 500°C.

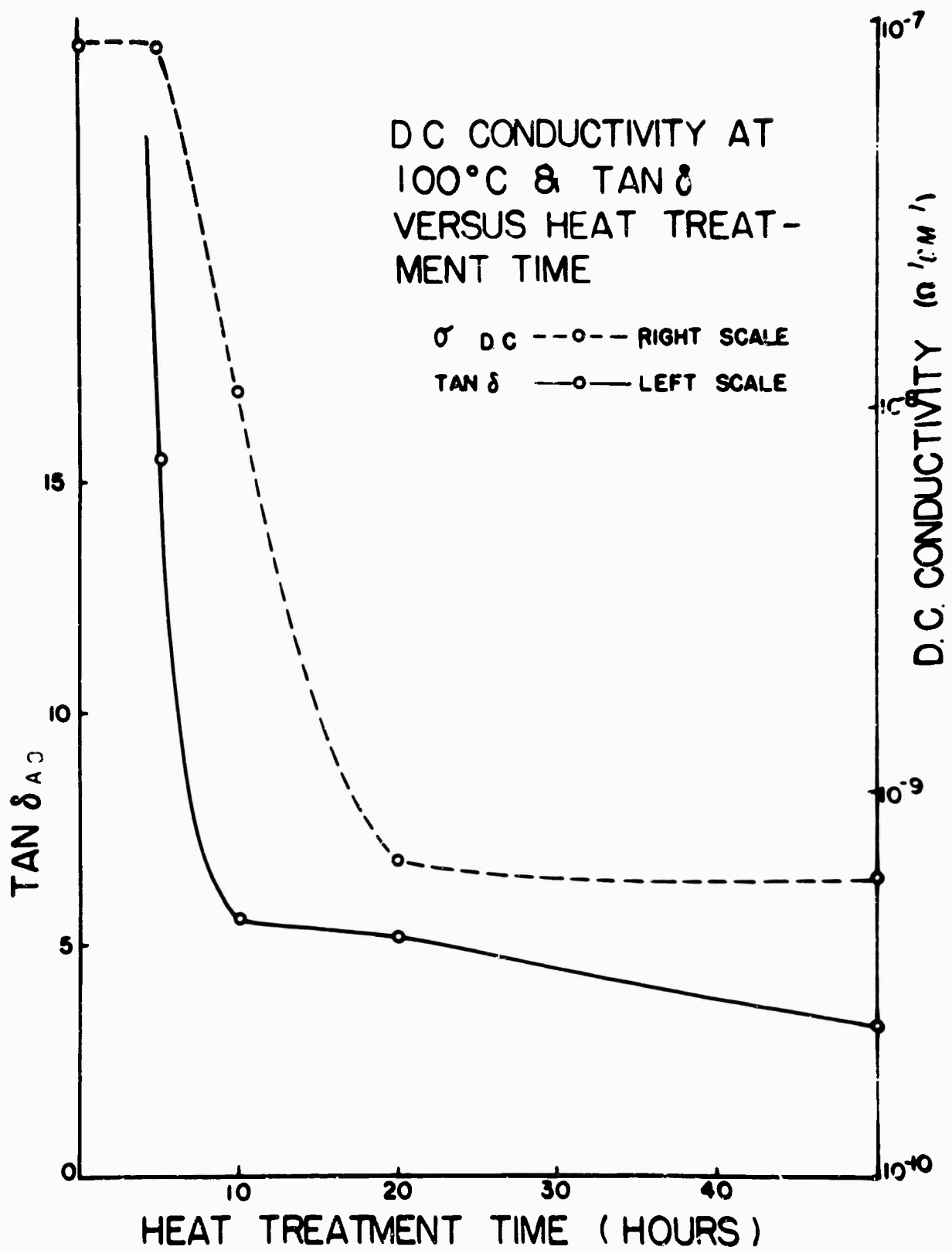


Fig. 5 Tan δ and dc conductivity versus heat treatment time at 500°C.

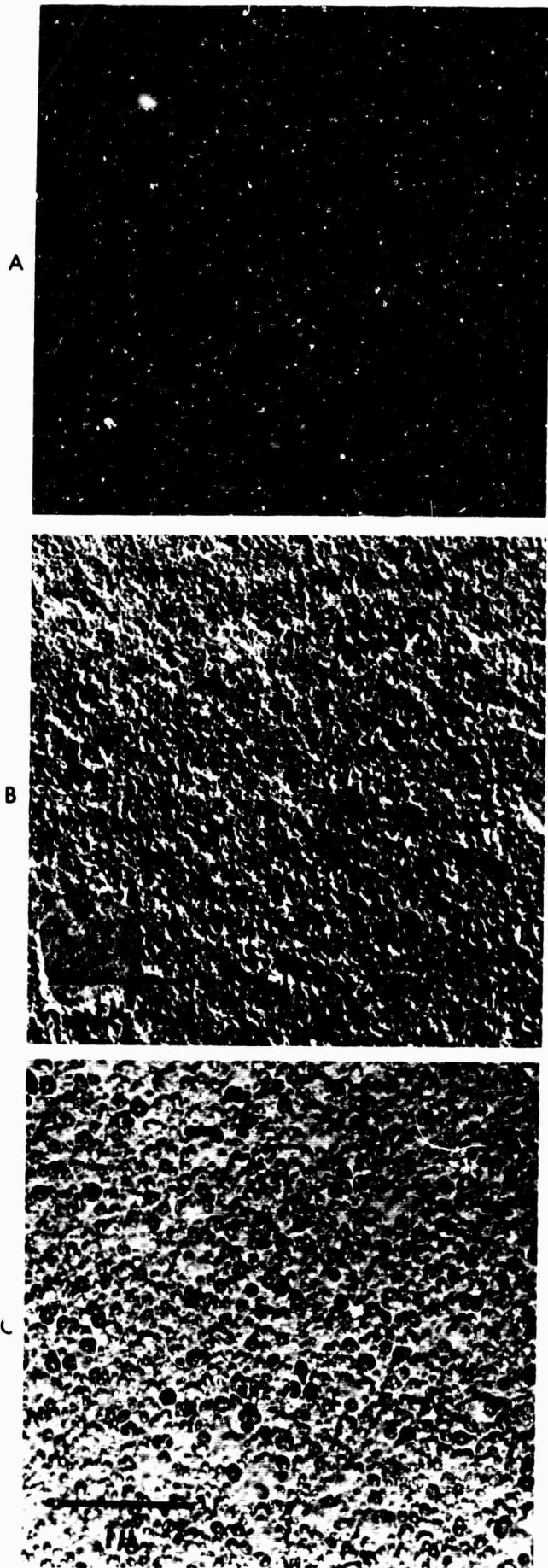


Fig. 10 Electron micrograph of the 17.5 weight % glass:
(a) as cast (b) 5 hours at 500°C (c) 50 hours at 500°C

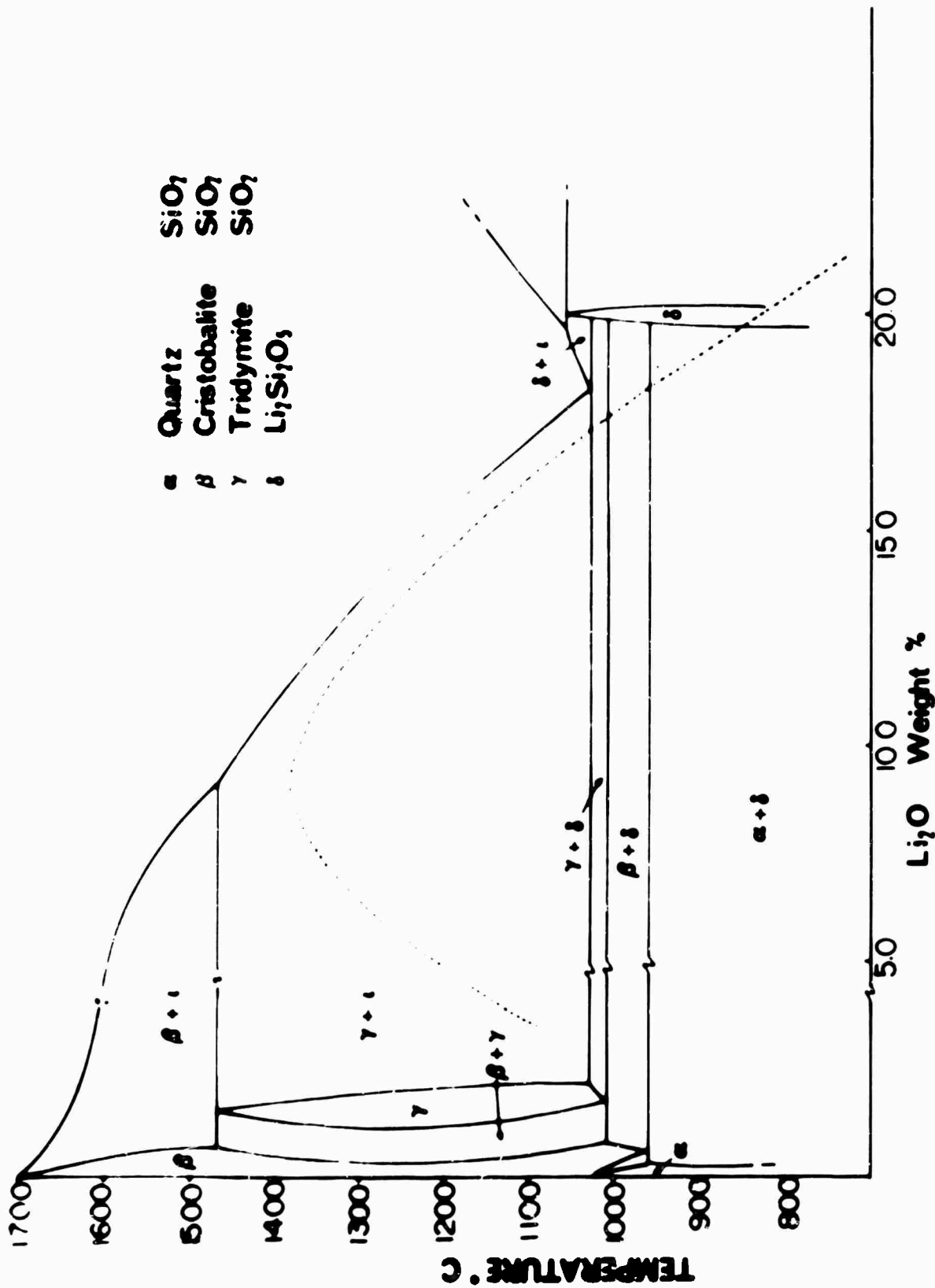
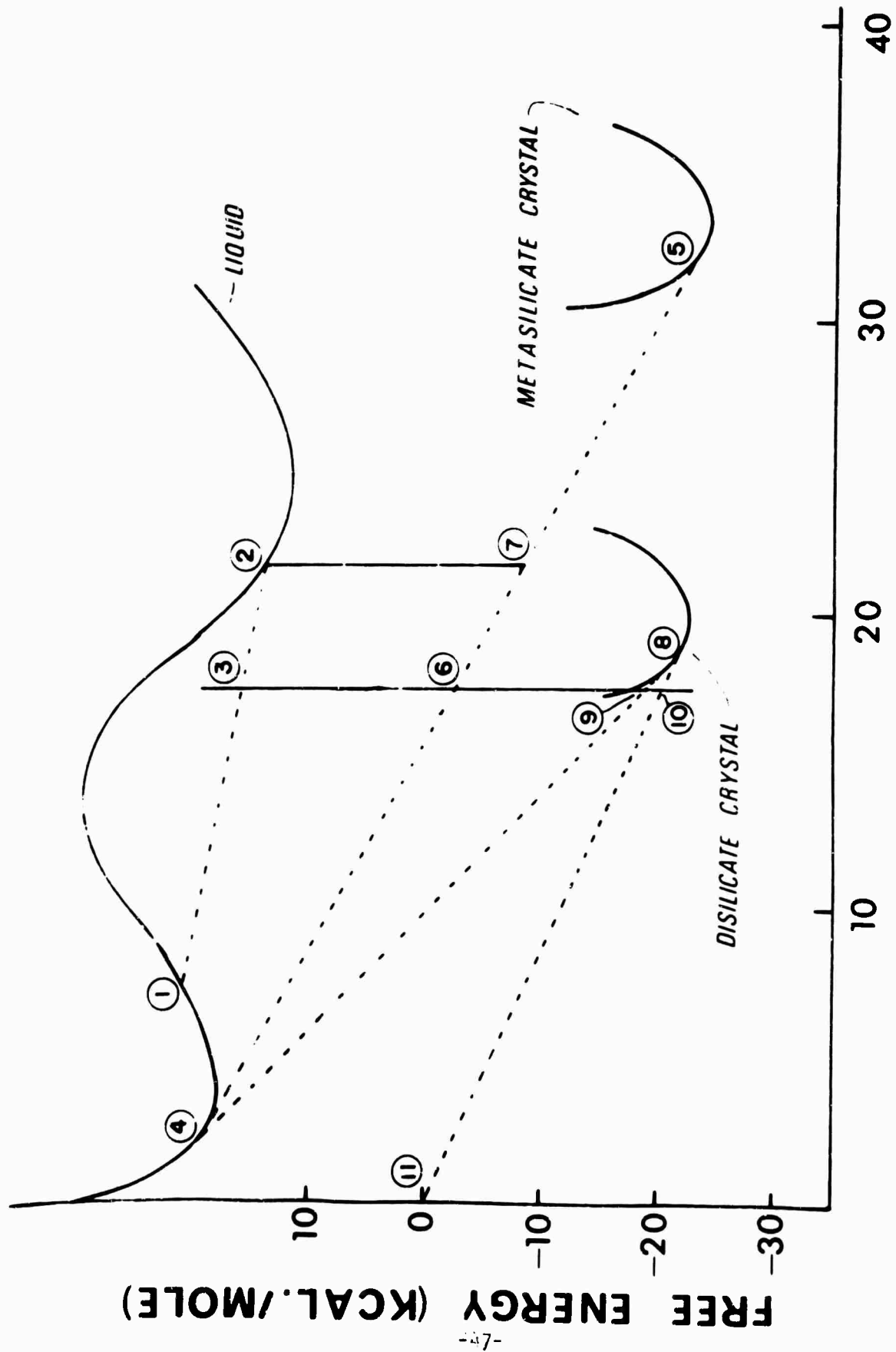


Fig. 11 Phase diagram of the $\text{Li}_2\text{O}-\text{SiO}_2$ system, after Kracek and Holmquist.²¹



COMPOSITION (WT. PER CENT)

Fig. 12 Free energy composition diagram at 500°C for the $\text{Li}_2\text{O-SiO}_2$ system.

III. SEMICONDUCTORS AND SEMICONDUCTOR DEVICES

(F.A. Lindholm, S.S. Li, R.W. Gould, J.J. Hren, L.L. Hench, E.R. Chenette, C.T. Sah)

Through experimental and theoretical studies, this program seeks to correlate electronic and quantum parameters of semiconductors with parameters describing structure and structural disorder. For each material under investigation, the studies concentrate on the relationship that impurity concentration bears to these parameters through the entire doping range: dilute, near-degenerate, and degenerate semiconductors. The electronic and quantum parameters of interest are those that relate to device design:

- a. collision cross-sections, mobility, diffusivity
- b. energy levels and degeneracies of defect centers
- c. emission and capture cross-section of defect centers; recombination, generation, and trapping
- d. band structure

The tools used to measure these parameters include the Hall and magnetoresistance experiments, various optical experiments (photovoltaic-junction, photoconductivity, Haynes-Shockley), the measurement of noise spectra, and conductivity-frequency-temperature experiments.

For each of these electronic and quantum parameters, correlation will be sought with such structural parameters as those describing:

- a. crystallographic perfection
- b. spatial distribution of impurity atoms; clustering
- c. pairing among impurity atoms (for example, between phosphorous and gold)
- d. imperfections; dislocations and vacancies

Field-ion and electron microscopy, analysis by the electron microprobe and analysis by x-ray scattering will be combined to yield these structural parameters. Theoretical studies will proceed in parallel with the experimental investigations, as will studies concerning the effects of irradiation.

The research reported here includes the results of both theoretical and experimental studies. Section A below concerns a theoretical study of the generalized Einstein relation that holds for degenerate as well as non-degen-

erate semiconductors. (This work has formed the basis for a paper, by F.A. Lindholm and R.W. Ayers, accepted for publication in the Proceedings of the IEEE). Section B reports the computer simulation of surface defects in diamond cubic structures, which is intended to enable the quantitative interpretation of field-ion-microscope images of silicon, germanium, and other semiconducting elements and compounds. Section C describes experimental technique and some preliminary data relevant to the measurement by small-angle x-ray scattering of the clustering present among impurity atoms in degenerate silicon. Section D outlines briefly some preliminary theoretical results concerning near-degenerate pn junctions.

A. GENERALIZED EINSTEIN RELATION FOR DEGENERATE SEMICONDUCTORS
(F.A. Lindholm and S.S. Li)

Recent studies have investigated the relationship that degenerate carrier concentrations existing in MOS¹ and bipolar² transistors bear to the performance at the device terminals. In one such study, Hachtel and Ruehli have demonstrated that, to accurately estimate the speed of modern switching transistors, one must take account of the degeneracy present in the emitters of these devices.² The conventional methods of analyzing semiconductor devices ignore degeneracy.

One aspect common to the conventional methods of analysis is the use of the Einstein relation³

$$D/\mu = kT/e \quad (1)$$

which, for a semiconductor at temperature T , states that the ratio of the transport parameters, D (diffusivity) and μ (mobility), is a constant of nature, this constant being the ratio of the thermal energy kT and the electron charge e . The Einstein relation, in the form expressed in eqn (1), is valid individually for each of the two carrier species: holes and electrons. In this conventional form, however, the relation holds true only for non-degenerate semiconductors, although its validity has been suggested, erroneously, for degenerate semiconductors.⁴

This research examines the generalized Einstein relation that holds for degenerate as well as for non-degenerate semiconductor material. To facilitate its use in device design, we set forth asymptotic and middle-range approximations and then utilize these approximations to plot the D/μ ratio as a function of carrier concentration. For any level of concentration, the resulting graph affords a comparison with the constant value of D/μ predicted by eqn (1), the conventional Einstein relation, and displays the error deriving from misuse of

of this relation.

The generalized Einstein relation, expressed in terms of the chemical potential ζ , is given by⁵

$$D/\mu = (1/e) \frac{d\zeta(n)}{d \ln n} \quad (2)$$

which states that, in general, the D/μ ratio depends on the carrier concentration n , rather than being constant. Eqn (2) holds for all levels of concentration, provided one accepts the validity for degenerate material of the conventional approximation that the density of quantum states varies as the square root of energy.⁶

To enhance the practical utility of the generalized Einstein relation, we shall approximate eqn (2) for three ranges of carrier concentration: non-degenerate ($n \ll N$, in which N denotes the effective density of states), near-degenerate ($n \sim N$), and high-degenerate ($n \gg N$). For non-degenerate concentrations, eqn (2) reduces to the classical Einstein relation, given in eqn (1).⁵ For near-degenerate concentrations, one can calculate $\zeta(n)$, and hence D/μ as a function of n , by use of approximate analytical expressions for Fermi integrals, which are given by Blakemore.⁷ For high-degenerate concentrations, eqn (2) reduces to⁵

$$D/\mu = (1/3) (1/e) (3/8\pi)^{2/3} (h^2/m^*)^{-2/3} n^{2/3}$$

in which h denotes Planck's constant, and m^* denotes the effective mass.

Fig. 1 shows the dependence of the D/μ ratio on n , constructed by application of these approximations and by use of published values for effective mass.⁸ For contrast, the figure displays the constant value of D/μ predicted by eqn (1). For holes in silicon, as an example, notice that the conventional Einstein relation starts to fail at a density of approximately $4 \times 10^{18} \text{ cm}^{-3}$; at a density of $2 \times 10^{20} \text{ cm}^{-3}$, the error introduced by use of this conventional relation exceeds a factor of five.

ALTERNATIVE FORMULATION

The foregoing treatment, based on an expression for the D/μ ratio in terms of the chemical potential, required the use of approximations for Fermi-Dirac integrals for different ranges of concentration and involved a lengthy, though straightforward, computation. It is possible, however, to derive an expression for the D/μ ratio in terms of tabulated functions; use of this expression enables quick construction of the D/μ dependence on concentration for any temperature and material. For the special cases of silicon and germanium at room temperature, the results reduce to those of Figure 1.

The derivation proceeds from the principle of detailed balance, which states that in thermal equilibrium the current density of electrons, for example, must vanish. Thus

$$\frac{D}{\mu} = \left(\frac{1}{e}\right) \frac{\frac{n}{\partial n}}{\frac{\partial x}}{\frac{\partial E_C}{\partial x}} = -\frac{1}{e} \frac{\frac{n}{dn}}{dE_C} \quad (3)$$

in which n denotes electron density; e , the magnitude of electron charge; E_C , the energy at the bottom of the conduction band; and x , a spatial coordinate. But

$$n = N_C F_{\frac{1}{2}}(\eta) \quad (4)$$

where

$$N_C = 2 \frac{2\pi m kT}{h^2}^{3/2}$$

and where

$$F_j(\eta) = \frac{1}{\Gamma(j+1)} \int_0^{\infty} \frac{\epsilon^j d\epsilon}{1 + \exp(\epsilon - \eta)} \quad (5)$$

are the Fermi-Dirac integrals,⁹ and $\eta = (E_F - E_C)/kT$ denotes the difference between the Fermi level and the lowest energy in the conduction band, this difference being normalized with respect to the thermal energy kT . Differentiation of eqn. (4) yields

$$\frac{dn}{dE_C} = -\frac{N_C}{kT} F_{-\frac{1}{2}}(\eta) \quad (6)$$

and substitution into eqn. (1) gives

$$\frac{D}{\mu} = \frac{kT}{e} \cdot \frac{F_{\frac{1}{2}}(\eta)}{F_{-\frac{1}{2}}(\eta)} \quad (7)$$

Eqn.(7) holds also for holes if one interprets η as $(E_v - E_F)/kT$, the normalized difference between the Fermi level and the highest energy in the valence band. Moreover, by a straightforward argument utilizing properties of the Fermi-Dirac integrals, one can demonstrate the equivalence of eqn (7) and eqn. (2).

Eqn. (7) and tables¹⁰ for the Fermi-Dirac integrals provide a direct means for displaying D/μ as a function of η , as in Fig. 2. Fig. 2 coupled with the graphical display of eqn. (2), given in Fig. 3, combine to yield Fig. 4 - which shows D/μ against carrier concentration for any temperature and for any material for which N_c , the effective density of states, can be evaluated. By examination of eqn. (2), one sees that this evaluation requires only the knowledge of the effective masses for holes and electrons for the material in question.

The basic approximation made here underlying the derivation of eqn. (7) and the construction of Figures 2 through 4 is that referred to previously: that the density of quantum states varies in the allowed bands as the square root of energy.^{6,11}

REFERENCES

1. T.I. Kamins and R.S. Muller, "Statistical considerations in MOSFET calculations," Solid State Electronics, Vol. 10, pp. 423-431, June 1967.
J.E. Schroeder and R.S. Muller, "Numerical calculations of the field distribution and related device parameters for MOS transistors in saturation," IEEE International Electron Device Meeting, Oct. 1967.
2. G.D. Hachtel and A.E. Ruehli, "The charge distribution in high-speed transistors," IEEE International Electron Device Meeting, Oct. 1967.
3. A. Einstein, Ann. Physik, vol. 17, pp. 549-559, 1905.
4. R.W. Lade, "The Einstein relation and Boltzmann boundary conditions in degenerate semiconductors," Proc. IEEE (Correspondence), vol. 52, pp. 743-744, June 1964. W. B. Berry, "A correction on the use of the Einstein relation in degenerate materials," Proc. IEEE (Correspondence), vol. 53, p. 188, Feb. 1965.
5. E. Spence, Electronic Semiconductors, pp. 293-295 and 384-385, McGraw-Hill, New York, 1958.
6. Ibid, pp. 384-385; cf. V.L. Bonch-Bruyevich, The Electronic Theory of Heavily Doped Semiconductors, pp. 65-76, American Elsevier Publishing Co., N. Y., 1966.
7. J.S. Blakemore, Semiconductor Statistics, Pergamon Press, N. Y. 1962, pp. 354-365.
8. E.M. Conwell, "Properties of silicon and germanium: II," Proc. IRE, Vol. 46, pp. 1281-1299, June 1958.
9. J.S. Blakemore, Semiconductor Statistics, New York: Pergamon Press, 1962, p. 79.
10. Ibid, pp. 346-353.
11. Ibid, pp. 355-357.

NOTE

The first portion of the research reported above is in press:

F.A. Lindholm and R.W. Ayers, "Generalized Einstein Relation for Degenerate Semiconductors," Proc. IEEE, April 1968.

The portion following ALTERNATIVE FORMULATION has been accepted for publication:

S.S. Li and F.A. Lindholm, "Alternative Formulation of Generalized Einstein Relation for Degenerate Semiconductors," Proc. IEEE.

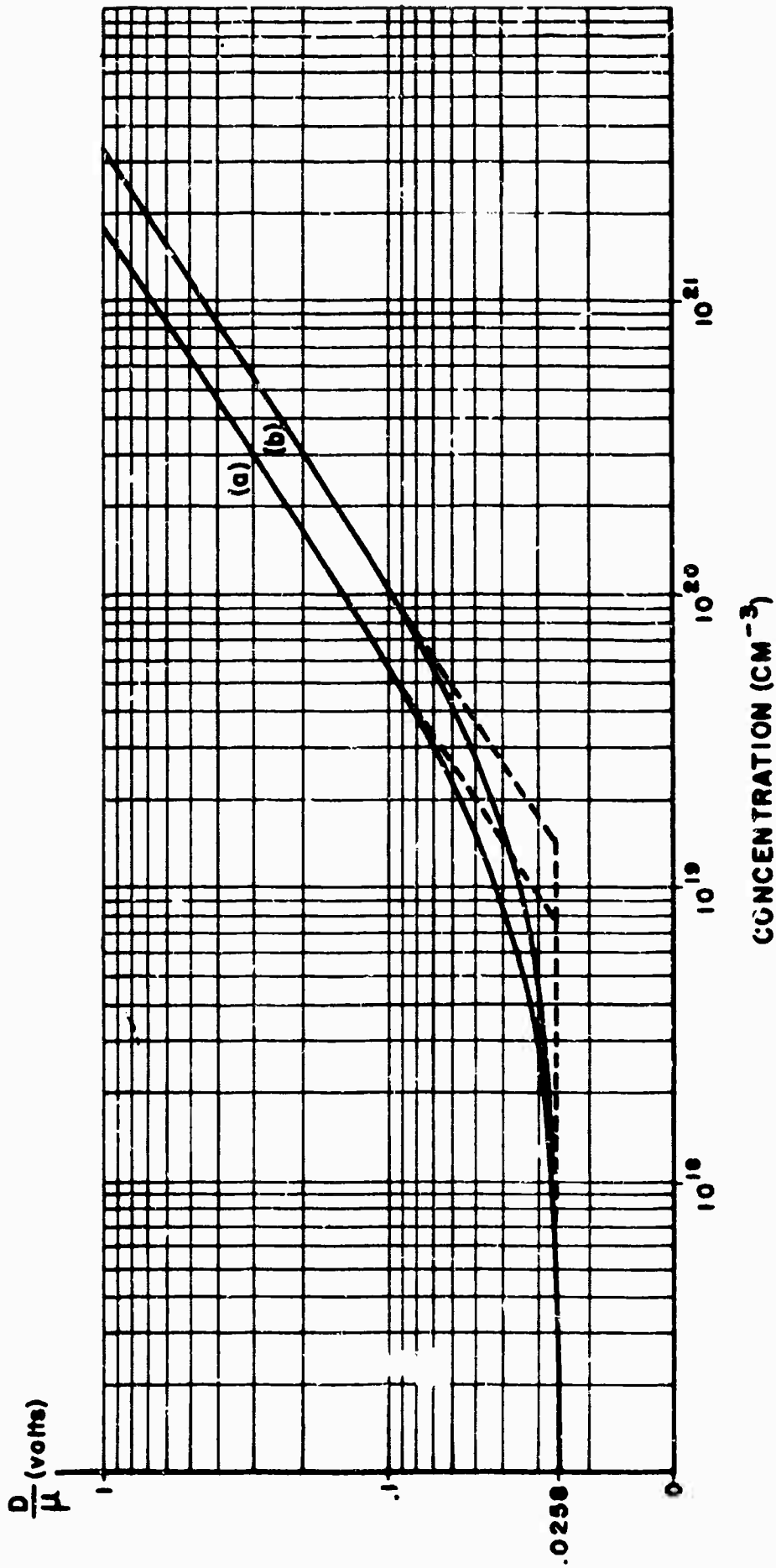


Fig. 1(a) Diffusivity-mobility ratio against concentration at 300°K for : (a) holes in Ge (b) electrons in Ge. The dotted lines show extrapolations of the low-concentration and the high-concentration asymptotes; the low-concentration asymptote is the conventional Einstein relation.

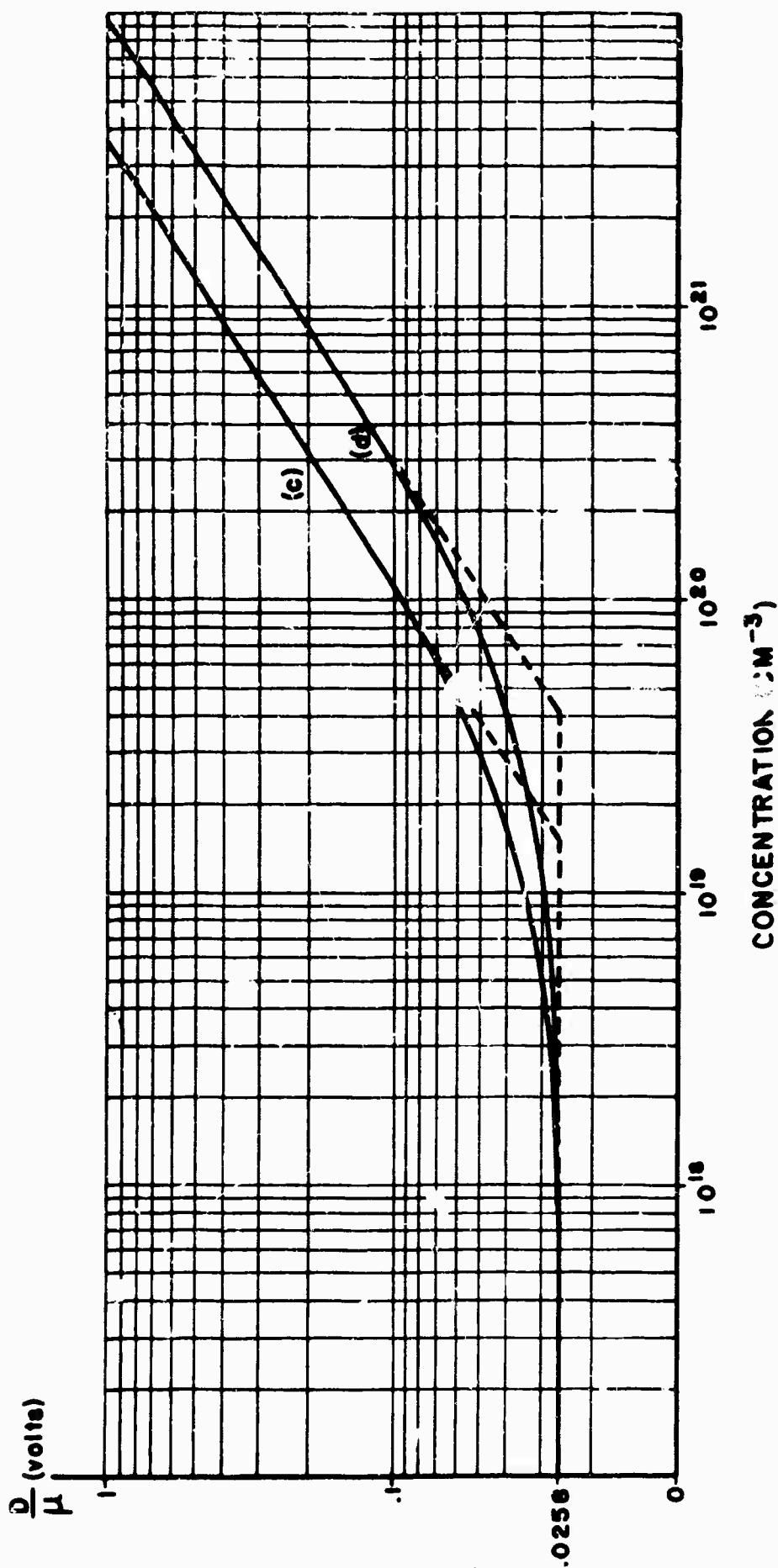


Fig. 1(b) Diffusivity-mobility ratio against concentration at 300°K for: (c) holes in Si, (d) electrons in Si. The dotted line shows extrapolations of the low-concentration and the high-concentration asymptotes; the low-concentration asymptote is the conventional Einstein relation.

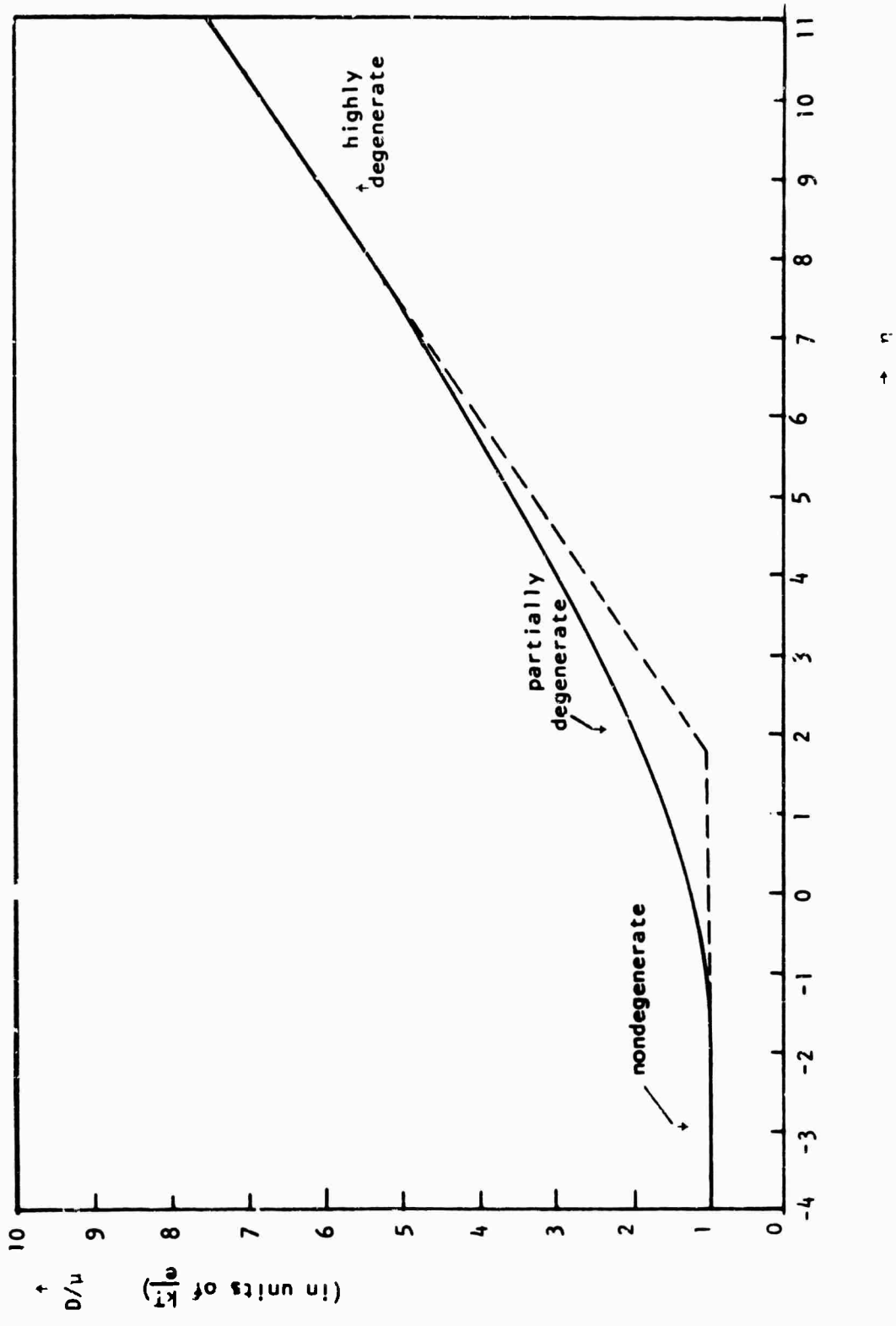


Fig. 2 Diffusivity-mobility ratio (D/μ) versus reduced Fermi energy (η).

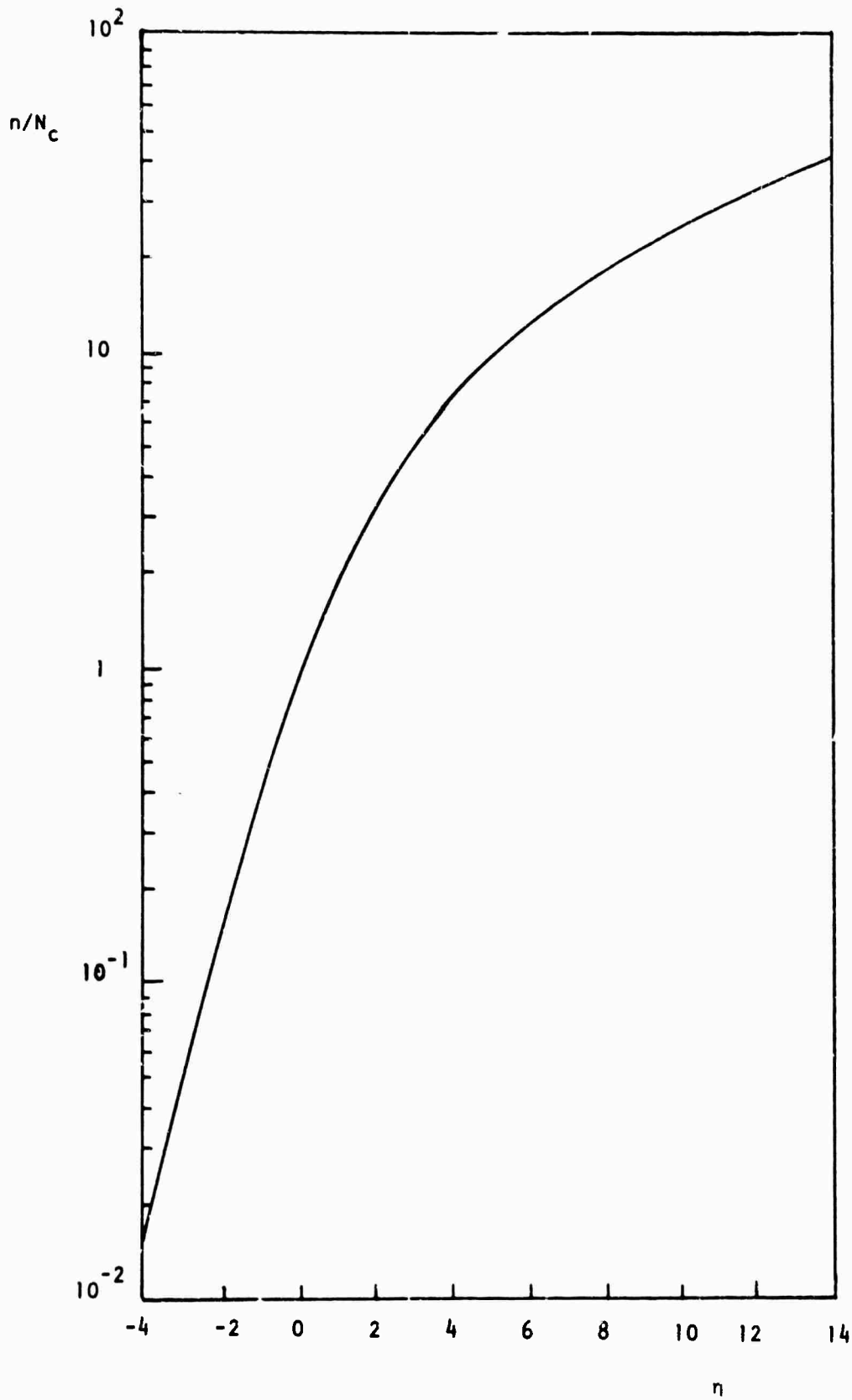


Fig. 3 Normalized carrier concentration (n/N_c) versus reduced Fermi energy.

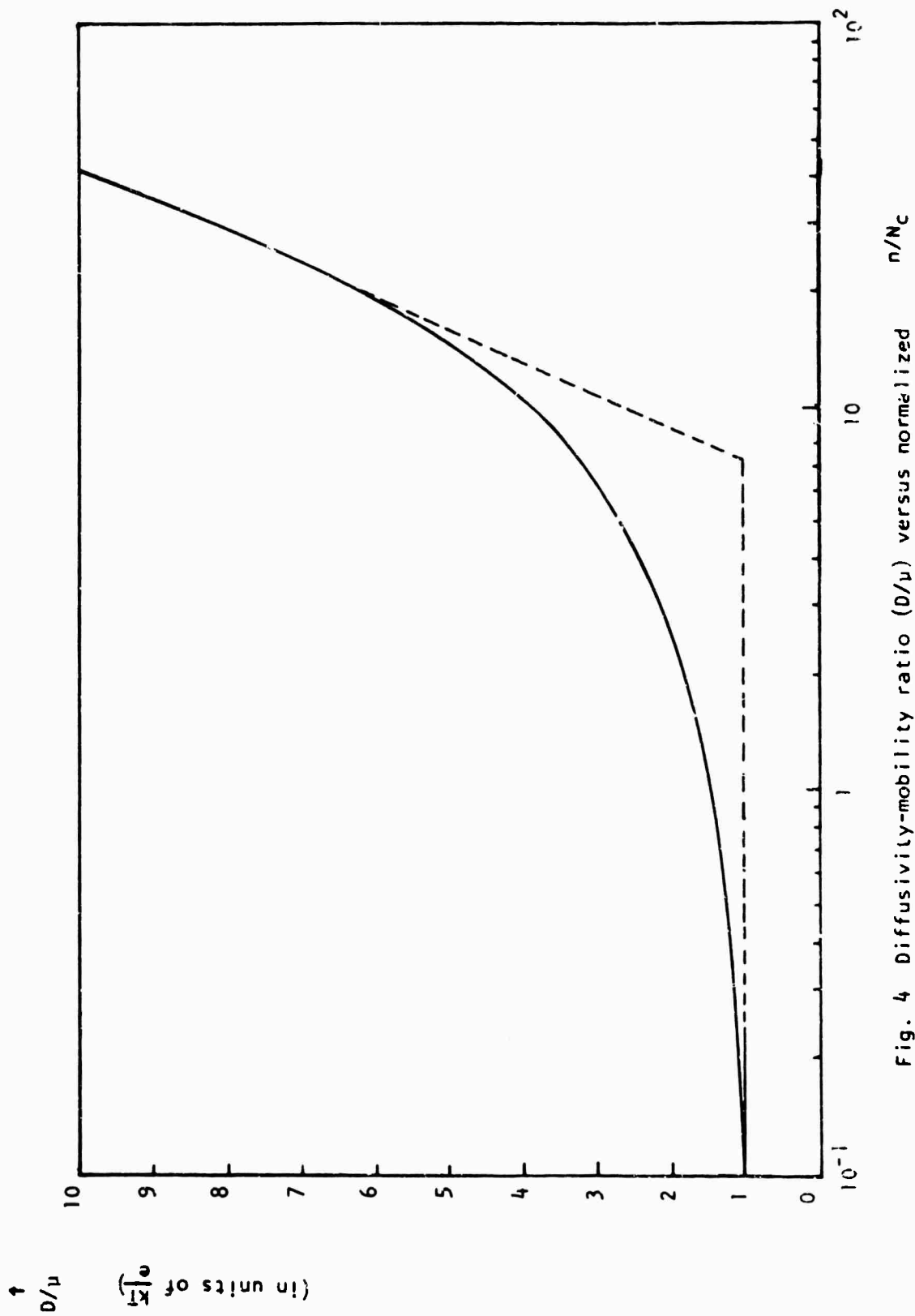


Fig. 4 Diffusivity-mobility ratio (D/μ) versus normalized carrier concentration (n/N_c).

B. COMPUTER SIMULATION OF SURFACE DEFECTS IN DIAMOND CUBIC STRUCTURES:
DISLOCATIONS INTERSECTING A SURFACE

(J.J. Hren)

Previous work from this laboratory (1-5) has demonstrated convincingly that single and multiple dislocations intersecting an arbitrary surface of a field emitter may be analyzed quantitatively via computer simulation techniques. Although the simulation procedure employed was rather a crude approximation, it served to illustrate the long-range effects of defects on a field-ion image. Agreement between experiment and the simulated defect images has been excellent to date, where the defect images studied have so far been limited to FCC, BCC and HCP structures, those commonly found in metals and alloys.

This work has now been extended to the diamond cubic structure which is more common in semiconducting elements and compounds. Because of the difference in binding, covalent vs metallic (for the earlier studies) there should be a pronounced change at the surface spirals produced in field emitters upon intersection by an arbitrary dislocation. We have so far not attempted to study the charge distribution, but have utilized only the simpler simulation procedure (shell model) used previously. One image of a simulated defect in diamond cubic is shown in Fig. 1.

Steps are now being taken to obtain actual images of silicon containing defects in the field-ion microscope. We have been somewhat delayed in our experimental studies by the move to new quarters, but are nearly ready to operate. While waiting for these facilities to be completed we are working on the more precise simulation procedure offered by the "neighbour model" approach which we had earlier shown to give point for point agreement with an actual image of tungsten. We should be able to get well along with the neighbour model approach for silicon during the coming quarter,

and also hope to have some experimental images in the near future. The only serious obstacle to obtaining good images of silicon is the low temperature conductivity, but heavy doping and evaporated conductive coatings of the specimens before imaging will overcome this obstacle, it is hoped. In any case electron emission studies may be conducted since they can be performed at higher temperatures. It is really too early to attempt to predict what the results will be at this stage, but the picture should be much clearer at the end of the next quarter.

REFERENCES

1. "Computer Simulated Ion-Emission Images of Dislocations: Screw Dislocation at the Center of [420]", R.C. Sanwald, S. Ranganathan and J.J. Hren, Applied Phys. Letters, 9 [11] (1966) 393.
"The Direct Observation of Individual Crystalline Dislocations," J.J. Hren, Proc. Fourth Space Congress, Cocoa Beach, Florida (April 3-6, 1967).
2. "Computer Simulation of Field Ion Images," R.C. Sanwald and J.J. Hren, Surface Science, 7 [2] (1967) 197.
"Fiber Optics in Field Ion Microscopy," J.J. Hren and R.W. Newman, Rev. Sci. Instr., 38, [7] (1967) 869.
"A Method for Indexing Field Ion Micrographs," R.W. Newman, R.C. Sanwald and J.J. Hren, J. Sci. Instr., 44 (1967) 828.
"Field Ion Microscopy of Mo Alloys," R.W. Newman and J.J. Hren, Phil. Mag., 16 [139] (1967) 211.
"The Effect of Crystal Symmetry on Field Ion Images of Ordered Alloys," R.W. Newman and J. J. Hren, Surface Science, 8 [4] (1967) 373.
"Growing Large single Crystals with Focused Light," S.D. Harkness, R.W. Gould, J.J. Hren and A.M. Sheble, Rev. Sci. Instr., 38 [11] (1967) 1676.
3. "Interpretation of Defects in Field Ion Images: FCC Materials," R.C. Sanwald and J.J. Hren, Surface Science, 9 [2] (1968) 257.
4. "Discussion on 'Structure of Surfaces and Their Interactions'", J.J. Hren, Proceedings NASA Symposium on Interdisciplinary Approach to Friction and Wear, San Antonio, Texas, November 28-30, 1967, pp. 1.1.1-1.1.30.
"A Critical Evaluation of X-ray Small angle Scattering Parameters by Transmission Electron Microscopy: GP Zones in Al Alloys," S.D. Harkness, R.W. Gould and J.J. Hren, Phil. Mag., Submitted for publication.
5. "An Electron Microscope and Field Ion Microscope Study of Defects in Quenched Platinum," R.W. Newman and J.J. Hren, phys. stat. sol., submitted for publication.

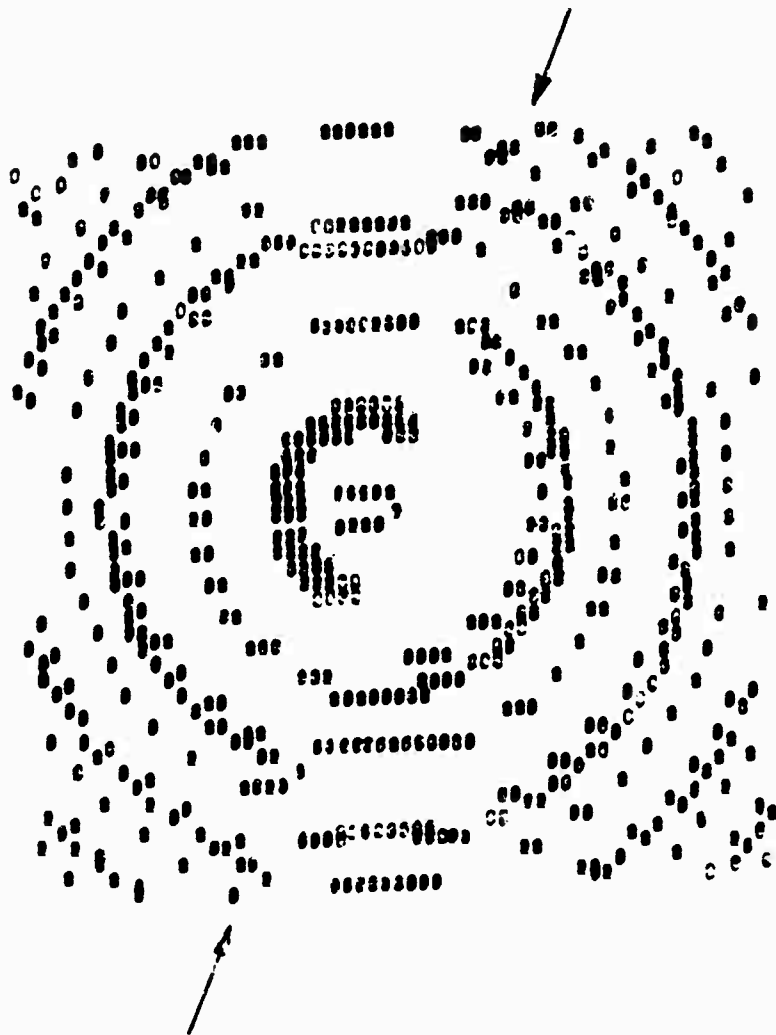


Fig. 1 Computer simulation of pure edge dislocation ($b=a/2[110]$) intersecting a spherical section near the (211) plane in a diamond cubic lattice. The effect may be described as a spiral with a clockwise sense and it leaves a ledge (along the arrows) of magnitude d_{211} .

C. DISTRIBUTION OF SOLUTE ELEMENTS IN DEGENERATE SEMICONDUCTORS
(R.W. Gould)

Evidence indicates that the solute elements in degenerate silicon may not be distributed randomly.¹ Although direct experimental observation is lacking, there is reason to believe that the impurity atoms will cluster, forming small regions rich in solute. Such clusters have been inferred from measured electrical properties.¹

The nature of these clusters (i.e., their size, shape, size distribution and number) and their effect on electrical properties of the host material form the basis of these investigations.

DETERMINATION OF SOLUTE DISTRIBUTION BY SMALL

ANGLE X-RAY SCATTERING

Small angle x-ray scattering has been used to study clustering in many metallic alloy systems.² Recently, this method has been extended to the study of low concentrations (1.2×10^{-5}) of vacancy clusters in radiation damaged metals.³ These latter investigations indicate that this method may provide a means to study the clustering of certain solute elements* in degenerate semiconductors. If the average cluster diameter is of the order of 10^2 angstroms and the number per unit volume is as great as 10^{15} to 10^{16} , then these clusters will give rise to measurable small angle scattering. The angular distribution of this scattering can be used to determine the size distribution and volume fraction of the clusters.

* Elements must be chosen such that the atomic number difference between the host and the impurity atom is large enough to produce small angle scattering. Adjacent elements on the periodic chart such as silicon and phosphorus would not be applicable.

SMALL ANGLE X-RAY SCATTERING FROM SILICON
CONTAINING ANTIMONY (10^{19} atoms per cm^3)

Experimental

Preparation of Samples

Samples must be thinned prior to examination by small angle x-ray scattering. The sample must be thinned to $\frac{1}{\mu}$ where μ is the linear absorption coefficient with respect to the radiation being used. The as-received samples were in the form of circular discs approximately one inch in diameter and from 0.3 to 0.8 millimeters thick. The specimens were cemented to a flat steel plate with a thermal setting cement and hand polished on metallographic polishing paper to a thickness of 0.12 to 0.18 millimeters. Small angle scattering patterns run on these specimens indicate the presence of a highly distorted layer on the Si surface giving rise to anomalously intense small angle scattering (double Bragg scattering). The distorted material was removed by etching in a mixture of 90% nitric-10% hydrofluoric acid. This treatment tended to remove most of the intense small angle scattering. An investigation is currently underway to determine the depth of the distorted layer produced by mechanical polishing.

Experimental Procedure

The polished samples were cut to size with a diamond scribe and masked off with a lead mask and placed in the holder of the small angle scattering Kratky camera. For the initial studies the small angle scattering was detected by scanning over the angular region of interest at a very slow speed. The scattering intensity is then obtained on a strip chart recorder as a function of scattering angle. Each sample was scanned with nickel and a cobalt balanced filter and the resulting intensity was corrected for sample absorption.

Sample absorption was measured by a standard method using an aluminum-zinc

scattering sample. A typical small angle scattering pattern of the silicon containing antimony (10^{19} atoms per cm^3) is shown in Fig. 1. The experimental parameters are indicated in the upper right-hand corner of this figure.

Experimental Results

These preliminary investigations indicate that this material is giving rise to some small angle x-ray scattering. It must now be determined how much of this scattering is due to retained mechanical work in the silicon specimen. This investigation is currently in progress. A sample of silicon is being polished as described above and etched in small steps. After each etching step, the sample is examined by the transmission Laue method to determine the nature and extent of the distortion. These initial studies have provided a valuable working background for the preparation of samples and the experimental conditions to be used with the Kratky small angle scattering camera.

We have placed an order with Alpha Crystals for a silicon sample containing approximately one-half of a percent by weight of antimony. This highly degenerate material will increase the probability of detecting the clusters if they are present. Until this material arrives, we will continue our investigations with the lower concentration crystals.

REFERENCES

1. C.T. Sah, personal communication.
2. R.W. Gould, "Applications of Small Angle Diffraction in Materials Research," Proceedings of the Fourth Space Congress (April 3-6, 1967)
3. V.K. Gerold, Small Angle X-ray Scattering, Gordon and Breach (1967) 277.

KRATKY CAMERA
 Si - 10^{19} Sb
 150 μ Entrance Slit
 50 kv. - 20ma.
 Cu Target - PHA
 Elevation Centroid
 1300 μ

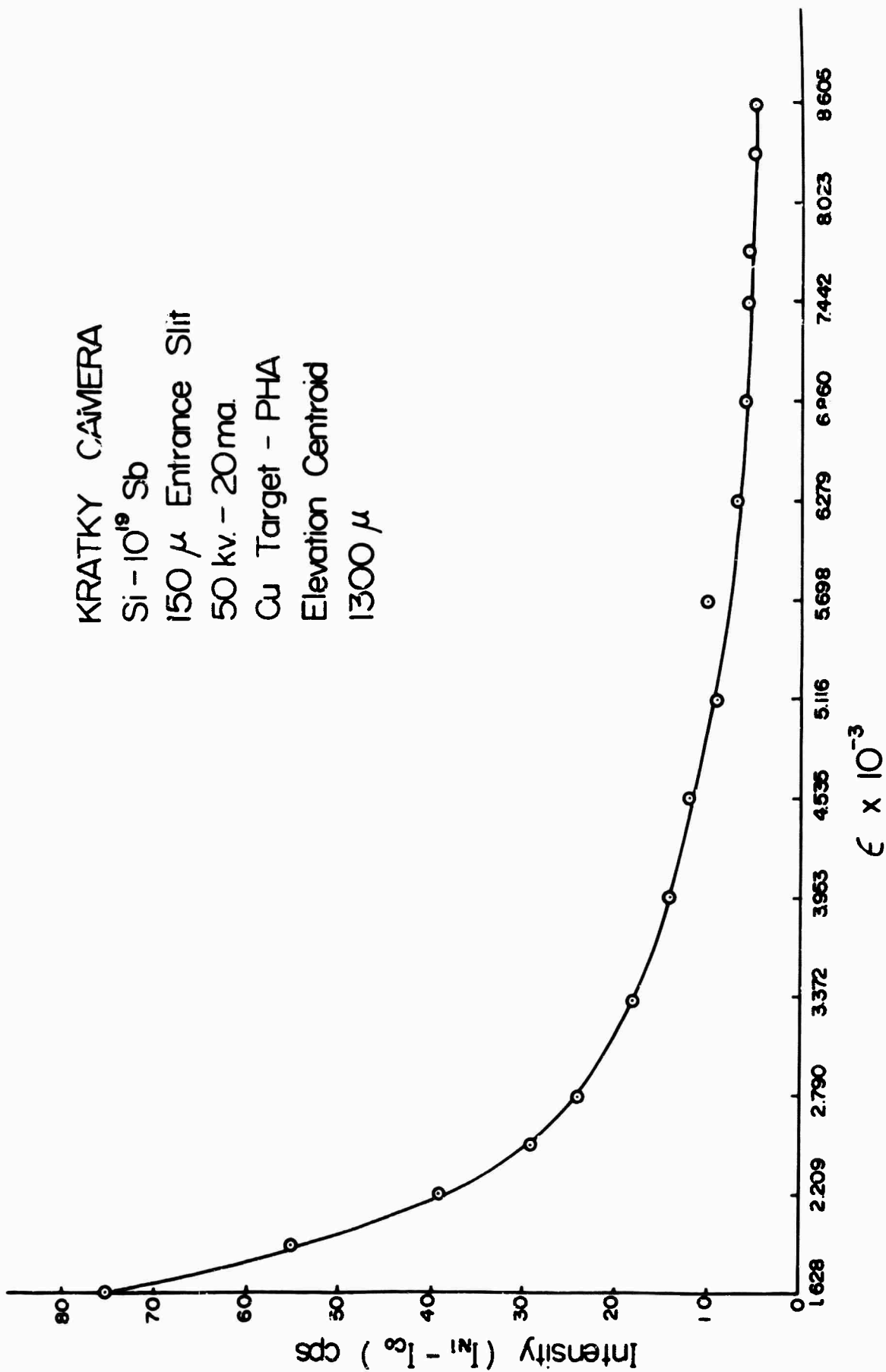


Fig. 1 Small angle x-ray scattering from a polished and etched sample containing 10^{19} atoms per cubic centimeter of antimony

D. TOWARD A THEORY OF NEAR-DEGENERATE PN JUNCTIONS
(F. A. Lindholm)

This research seeks to quantitatively describe the behavior of pn junctions having impurity densities in the near-degenerate range: densities between those for which Maxwell-Boltzmann statistics hold and those which yield heavily degenerate semiconductors. The present reporting describes briefly the approach being used and some tentative theoretical results.

The approach proceeds from the conventional theory¹ for non-degenerate pn junctions, extending it to the near-degenerate range of concentrations by eliminating or modifying approximations. The aim is to develop expressions of accuracy adequate for use in the design and analysis of near-degenerate junctions.

Thus far, the effort has yielded expressions for:

- (1) The contact potential as a function of impurity concentration
- (2) The electron-hole-density product at the edges of the space-charge region for applied voltages not exceeding ninety per cent of the contact potential.
- (3) The minority densities at the edge of the space charge region for applied voltages small enough that low-injection conditions prevail.

The approximations used in obtaining these results are:

- (1) constancy of the quasi-Fermi levels throughout the space-charge region.²
- (2) approximations of Fermi-Dirac integrals, accurate to within three per cent.³
- (3) immutability of band edge and impurity level in the near-degenerate range of concentrations.⁴

This research is now turning to the analytical assessment of the adequacy of approximations (1) and (3) above.

REFERENCES

1. A.K. Jonscher, Principles of Semiconductor Junction Device Operation, Wiley, New York, 1960; Ch. 4.
2. C.T. Sah, "The Spatial Variation of the Quasi-Fermi Potentials in PN Junctions," IEEE Trans. Electron Devices, Vol. ED-12, pp. 839-846; Dec. 1966.
3. J.S. Blakemore, Semiconductor Statistics, Pergamon Press, New York, 1962; pp. 354-365.
4. see, e.g., V.L. Bonch-Bruyevich, The Electronic Theory of Heavily Doped Semiconductors, American Elsevier, New York, 1966; pp. 65-76.

IV. RADIATION STUDIES (L.L. Hench)

The initial emphasis of the radiation program has been the evaluation of fast-neutron exposure on the conductivity and dielectric properties of semiconducting glasses and insulating glass-ceramics. The results of these experiments will determine to what extent glass properties can be modified by thermal treatment and still retain irradiation stability.

Semiconducting glass

The A.C. conductivity of a quenched $V_2O_5-KPO_3$ semiconducting glass is compared with the conductivity after a heat-treatment of 1/2 hour at $288^\circ C$ in Figure 1. The large change in conductivity with heat treatment has been attributed to the presence of small crystallites in the glass.⁽¹⁾ The conductivity of several $V_2O_5-P_2O_5$ glasses has previously been shown to be insensitive to neutron dosages of up to 4×10^{17} nvt.⁽²⁾ It was the objective of the present experiment to determine whether the electronic conductivity of a semiconducting glass altered by partial crystallization would also be insensitive to fast neutron dosages in the 10^{17} nvt range. The conductivity of the $V_2O_5-KPO_3$ glasses before and after irradiation is illustrated in Figure 1. It can be noted that the properties of the quenched glass is independent of the radiation exposure. The conductivity of the partially crystallized glass, however, appears to be slightly increased with the neutron exposure.

A similar increase in the conductivity of V_{205} - P_{205} glasses was observed by Hench and Daughenbaugh⁽²⁾ when the glasses were exposed to a γ -ray dosage of 1.2×10^8 rads.

The results of Figure 1 also indicate that the A.C. conductivity dispersion characteristic of semiconducting glasses⁽³⁾ has been partially restored by the 10^{17} nvt dosage. Theoretical interpretation of the results of these and larger irradiation dosages is currently in progress.

Glass-Ceramics

Previous investigations of the dielectric properties of Li_2O - SiO_2 glasses has revealed the presence of large loss peaks associated with metastable crystalline precipitates.⁽⁴⁾ Simultaneous with the appearance of the absorption peaks the D.C. conductivity decreased by a factor of 100. The metastable precipitates result from a thermal treatment of 5 hours at $500^\circ C$. The objective of the present experiment has been to determine the stability of the electrical properties of thermally treated insulating glasses.

The dielectric loss spectra of a thermally treated 17.5 weight percent Li_2O - SiO_2 glass is compared before and after a 1×10^{17} nvt fast neutron dosage in Figure 2. It can be seen that the heterogeneous loss peak is still present after fast neutron exposure. Consequently, it must be concluded that the crystallites present in the Li_2O - SiO_2 glass are stable at the dosage of this experiment. The small decrease in peak height may correspond to the initial stages of resorption of the metastable crystallites. Resorption of the crystallites has been shown previously to occur with exposure to a temperature of $500^\circ C$ for periods of 5-100 hours. Studies of larger neutron dosages are in progress to establish whether fast neutrons can produce a similar resorption.

REFERENCES

1. L.L. Hench, A.E. Clark, D.L. Kinser, "Electrical Properties of a Thermally Treated Semiconducting Glass," to be submitted to J. Am. Ceram. Soc.
2. L.L. Hench and G.A. Daughenbaugh, "Radiation Effects in Semiconducting Glasses," J. Nuclear Materials, in press.
3. L.L. Hench and D.A. Jenkins, "A.C. Conductivity of a Semiconducting Glass," Phys. Stat. Sol. 20, 327 (1957).
4. D.L. Kinser and L.L. Hench, "Effect of Metastable Precipitate on the Electrical Properties of a Lithia-Silicate Glass," J. Am. Ceram. Soc., accepted for publication.

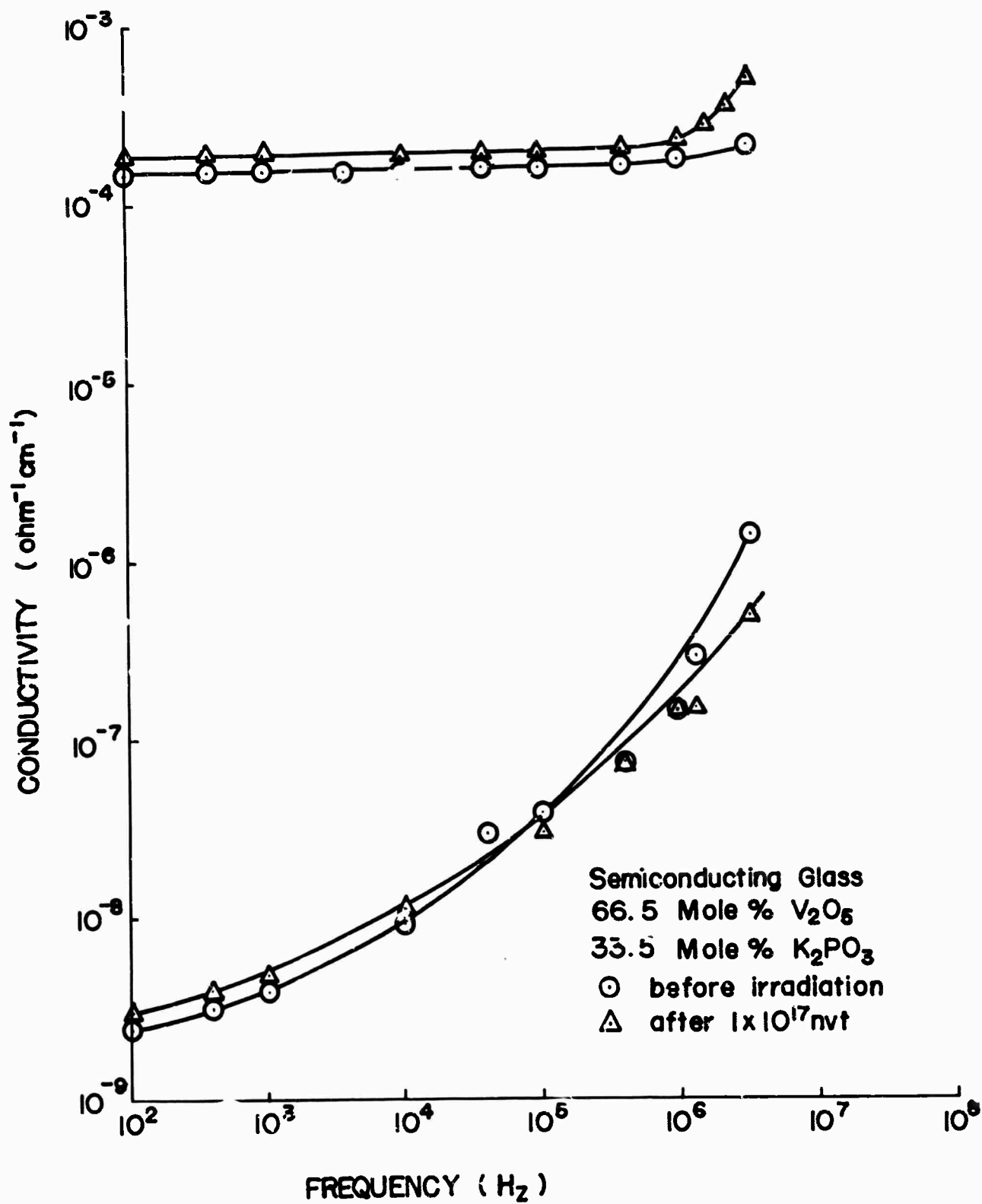
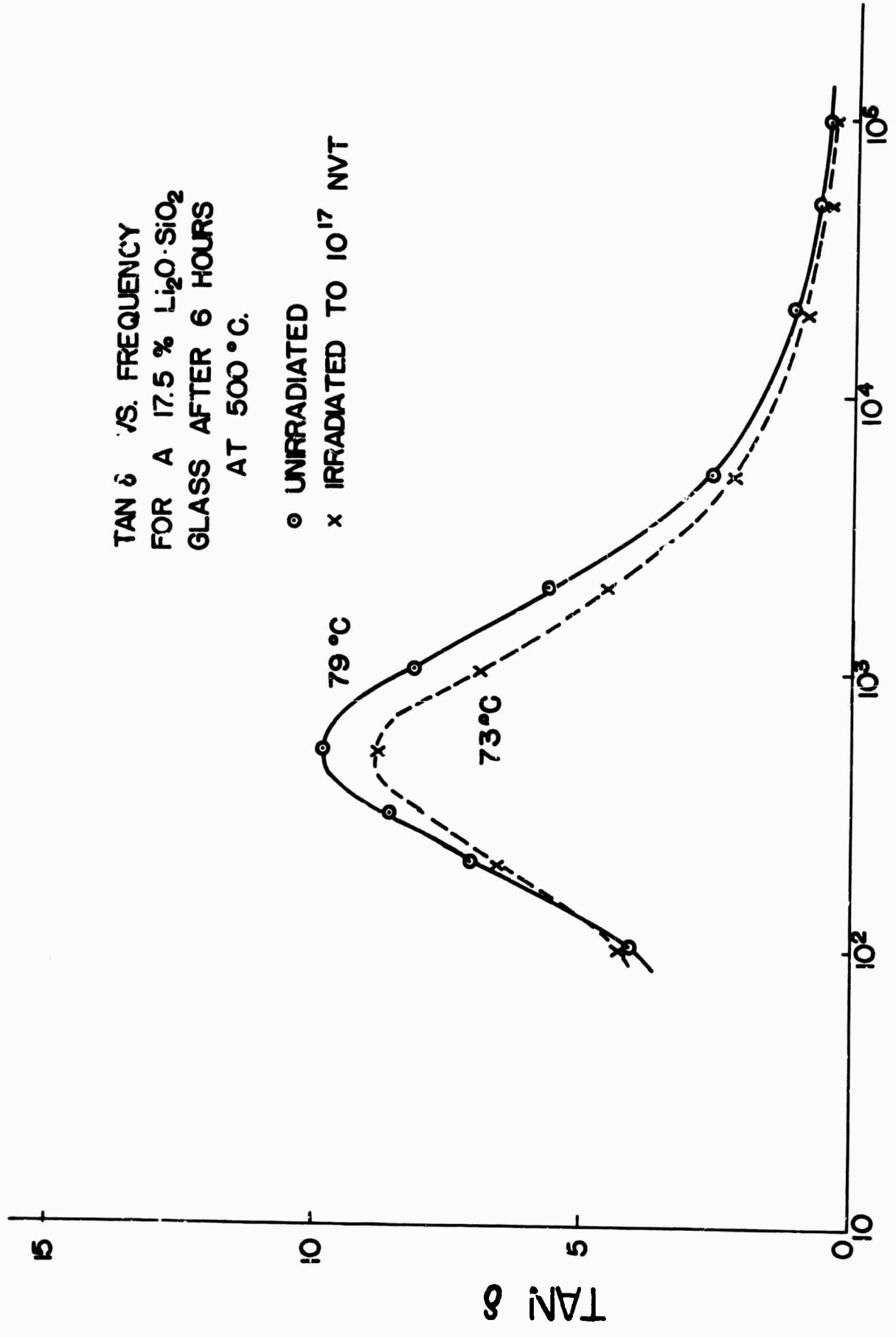


Fig. 1 Effect of neutron irradiation on the A.C. conductivity of a quenched semiconducting glass (low conductivity) and a thermally treated semiconducting glass (high conductivity).



FREQUENCY

Fig. 2 Effect of neutron irradiation on the loss angle of an insulating glass with metastable crystallites present.

V. NOISE STUDIES
(E.R. Chenette, A.J. Brodersen)

Several projects have been undertaken in the general area of noise studies. So far most of the work has been concerned with setting up the required test facilities and with the development of some specialized test fixtures and techniques. Some of the projects require the development - and successful fabrication - of special test devices or samples in the Solid State Fabrication Laboratory. A brief description of the initial phases of the noise program is presented here.

One project is the design and fabrication of a "low-noise" planar transistor. The goal is to exploit present knowledge of the sources of noise in transistors and to build a transistor with noise performance superior to any commercially available.

A second project is concerned with the study of sources of flicker noise in bipolar transistors. Pairs of identical transistors, fabricated on the same substrate, with field plates near the emitter-base junctions so as to permit control of the surface potential there, are being designed and will be built. It is expected that noise studies on these devices will yield some additional information about the relation between flicker noise and surface recombination near the emitter-base junction.

An improved method of measuring noise in bipolar transistors is being implemented. This involves measurement of the equivalent noise at both the input and the output of a transistor operating in common-emitter connection with source admittance as a parameter.

Closely related to the studies of noise in bipolar transistors is the investigation of the noise limitations of linear integrated circuits. The emphasis here is on possible differences in the noise performance of discrete devices and devices as found in typical planar monolithic technology. Cf

particular interest is possible electrical and thermal coupling of noise sources through the substrate.

Planar silicon Schottky-barrier diodes having a pn junction guard ring structure are being fabricated. Noise studies will be included as a part of the characterization of these devices.

Preparation of equipment for the measurement of noise spectra of materials in bulk form is underway. Samples of semiconducting glass are being prepared for these studies.

VI. LABORATORY FACILITIES

This section describes the major additions to our laboratory facilities made during the reporting period.

A. SOLID-STATE FABRICATION LABORATORY (A.J. Brodersen)

New laboratory facilities were occupied early in November. These laboratory facilities are part of a major expansion program in the College of Engineering. A floor plan of the new facility is shown in Fig. 1. This facility includes a complete capability for making semiconductor devices.

Major emphasis in the first half of the year has been spent in developing the capability of fabricating silicon planar devices and integrated circuits. (Thin film activities are reported in Section VI-C). Initial effort was devoted to fabricating planar double-diffused bipolar junction transistors since the fabrication of this device requires all the major processing steps and since the bipolar transistor is the most commonly used device in silicon integrated circuits.

Fig. 2(a) shows a photomicrograph of a typical transistor fabricated in this laboratory. All fabrication steps, with the single exception of crystal growth, were done here. These steps include mask making, photolithography, and diffusion. Fig. 2(b) shows the common-emitter characteristics of a typical device. Good uniformity was obtained among devices on the same silicon wafer, and successive runs have indicated good reproducibility of devices.

Typical characteristics are:

$$h_{FE} = 50 - 100$$

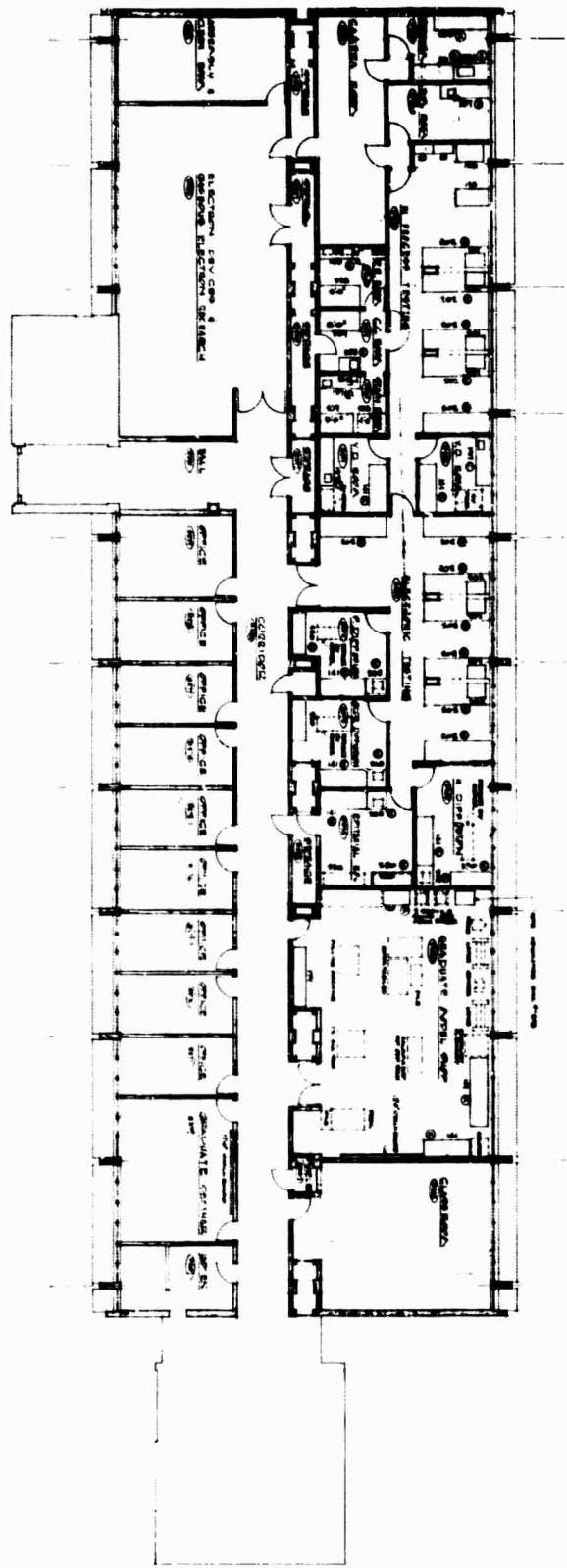
$$BV_{CBO} = 60 \text{ V}$$

$$BV_{CEO} = 25 \text{ V}$$

$$BV_{BE0} = 6.5 \text{ V}$$

The devices now being made have base widths of 0.8 microns. A complete ac characterization has not as yet been made.

The progress to date has been encouraging. The fabrication facilities are now capable of making excellent devices.



REVISED SECOND FLOOR PLAN
 DATE: 11/15/54
 DRAWN BY: J. J. JACOBSON
 CHECKED BY: J. J. JACOBSON

SCHEDULE OF LABORATORY EQUIPMENT AND SUPPLIES
 Data showing quantity of the items and their location.

Room No.	Quantity	Description	Location
207	1	Refrigerator	Lab. 207
208	1	Refrigerator	Lab. 208
209	1	Refrigerator	Lab. 209
210	1	Refrigerator	Lab. 210
211	1	Refrigerator	Lab. 211
212	1	Refrigerator	Lab. 212
213	1	Refrigerator	Lab. 213
214	1	Refrigerator	Lab. 214
215	1	Refrigerator	Lab. 215
216	1	Refrigerator	Lab. 216
217	1	Refrigerator	Lab. 217
218	1	Refrigerator	Lab. 218
219	1	Refrigerator	Lab. 219
220	1	Refrigerator	Lab. 220
221	1	Refrigerator	Lab. 221
222	1	Refrigerator	Lab. 222
223	1	Refrigerator	Lab. 223
224	1	Refrigerator	Lab. 224
225	1	Refrigerator	Lab. 225
226	1	Refrigerator	Lab. 226
227	1	Refrigerator	Lab. 227
228	1	Refrigerator	Lab. 228
229	1	Refrigerator	Lab. 229
230	1	Refrigerator	Lab. 230
231	1	Refrigerator	Lab. 231
232	1	Refrigerator	Lab. 232
233	1	Refrigerator	Lab. 233
234	1	Refrigerator	Lab. 234
235	1	Refrigerator	Lab. 235
236	1	Refrigerator	Lab. 236
237	1	Refrigerator	Lab. 237
238	1	Refrigerator	Lab. 238
239	1	Refrigerator	Lab. 239
240	1	Refrigerator	Lab. 240
241	1	Refrigerator	Lab. 241
242	1	Refrigerator	Lab. 242
243	1	Refrigerator	Lab. 243
244	1	Refrigerator	Lab. 244
245	1	Refrigerator	Lab. 245
246	1	Refrigerator	Lab. 246
247	1	Refrigerator	Lab. 247
248	1	Refrigerator	Lab. 248
249	1	Refrigerator	Lab. 249
250	1	Refrigerator	Lab. 250

ENGINEERING EXPANSION UNIVERSITY OF FLORIDA GAINESVILLE, FLORIDA

McELVY & JENNEWAIN ARCHITECTS AIA FORREST M. KELLEY, JR. AIA D. NEIL WEBB AIA
 RANDOLPH C. JACKSON, III, INC. CONSULTING ENGINEER BRANCH & OETHE CONSULTING ENGINEERS
 ELECTRICAL ENGINEERING BY J. J. JACOBSON
 DRAWING NO. 2000 JOB NO. 519
 E.E.L. EQUIPMENT PLANS

Fig. 1 -78-

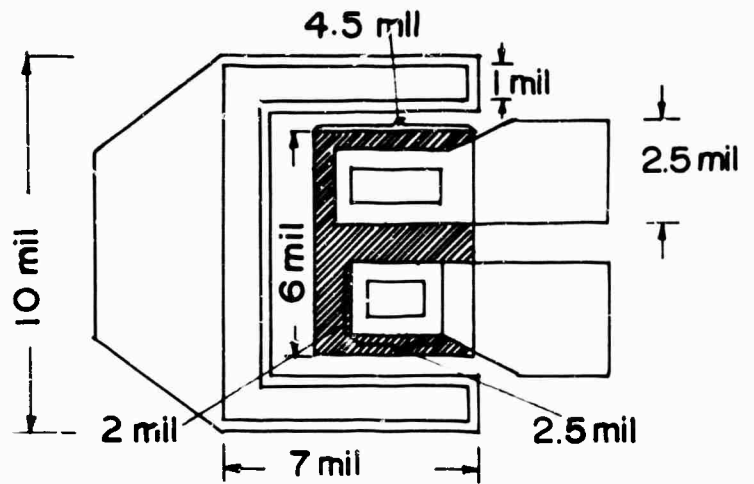
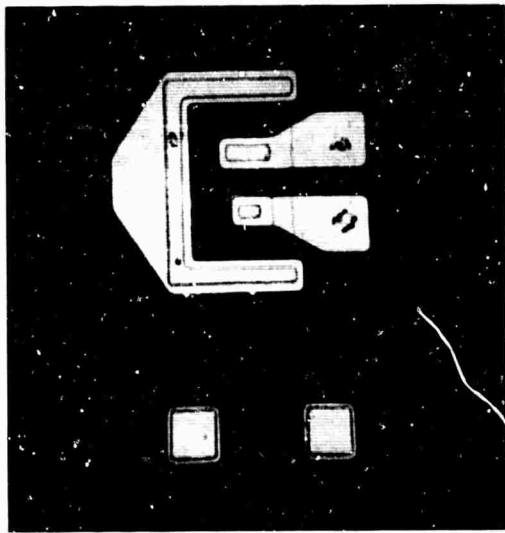
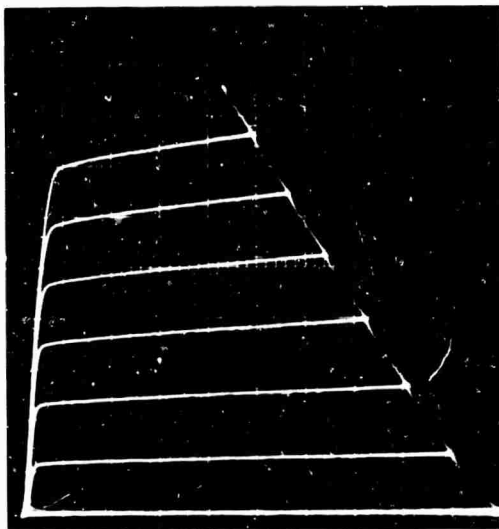


Fig. (2a) PLAN VIEW OF TRANSISTOR



Vertical scale
1m A / division

Horizontal scale
1V / division

.01 mA of base
current / step

Fig. (2b) I_c VS V_{ce}

B. MODIFICATION OF ELECTRON MICROPROBE
(R.W. Gould)

Observation of Specimens with Back-Scattered Electrons

Specimens may be observed in the electron microprobe by scanning the beam over a small area on the specimen surface and monitoring the results of the electron-sample interaction. This interaction may be observed in several ways; i.e., characteristic x-ray images of the area scanned by the beam, sample current images (electron drain-off as a function of beam position), back-scattered electron fraction as a function of position. This latter mode may be subdivided into two categories: primary back-scattered electrons, those possessing energies approximately the same as the incident beam (10 to 20 KEV), and secondary back-scattered electrons, those produced in the sample but with a much lower energy than the primary beam. The energies of the secondary electrons will be affected by the work function of the material as well as the local electrical potentials in the material. Thus the study of the spatial distribution of back-scattered secondary electrons can provide a means of analysis for materials, devices, and integrated circuits.¹

A secondary electron detector has been added to the microprobe in the Department of Metallurgical and Materials Engineering (see Fig. 1) by Alton Electronics, Inc. according to the design given by Potts.² The development of this device is currently in progress. Provisions have been made to detect secondary back-scattered electrons in flat and stereo modes. The latter feature produces a three-dimension appearance in the image and clearly shows surface contours and irregularities. The representative results are shown in Figs. 2 through 8. Figs. 4 and 5, taken from Potts' paper,² show the effect of an increased bias current on a microcircuit.

REFERENCES

1. C.C. Nealby and C.W. Laakso, "Planar Silicon Device Failure Mechanism Studied with a Microanalyzer Electron Probe," Physics of Failure in Electronics, 3, RADC (1965).
2. H.R. Potts, "Secondary Electron Analysis of Electronic Microcircuits," Microelectronics and Reliability, Pergamon Press 6 (1967) 173-175.

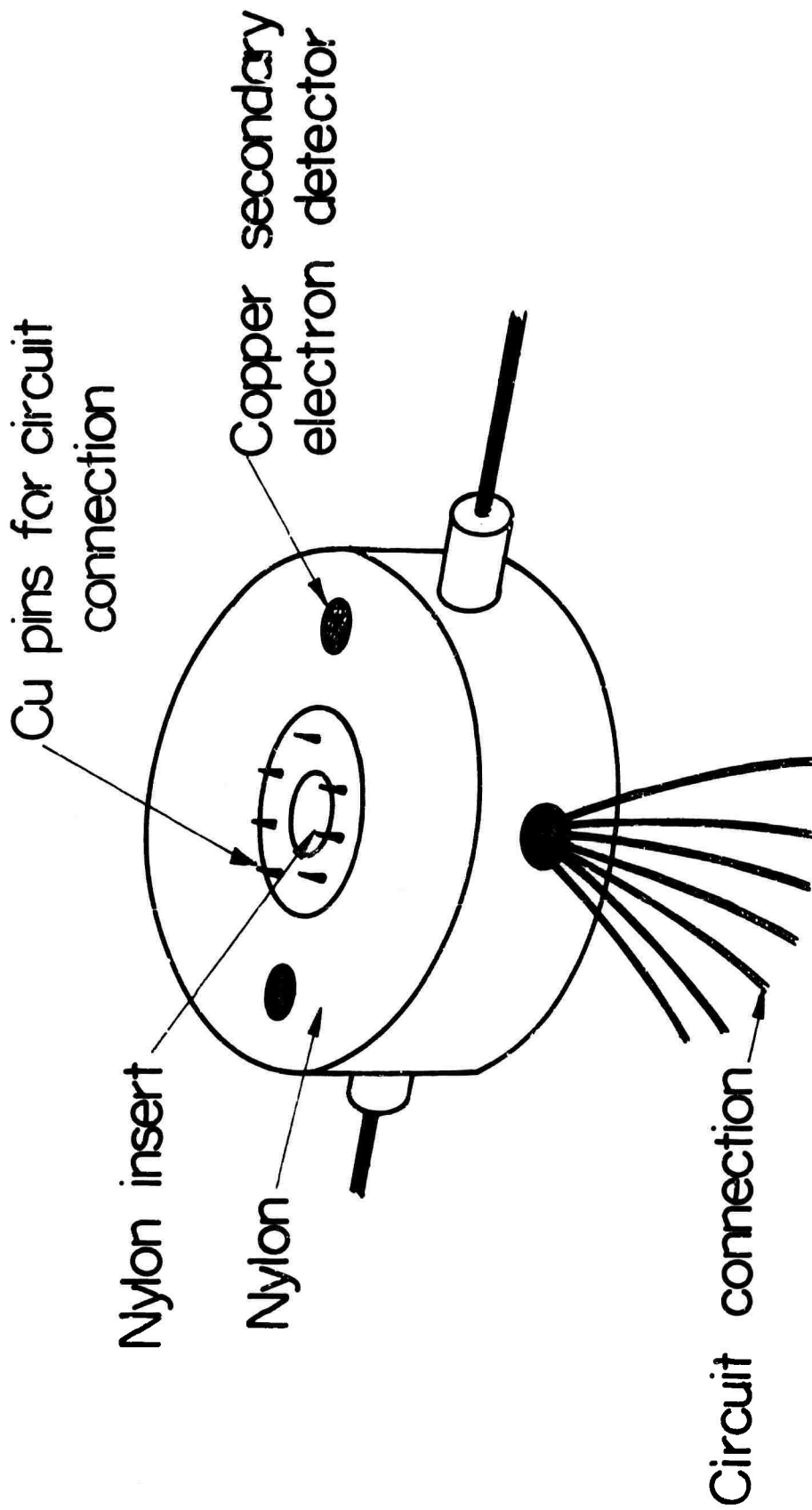


Fig. 1 Schematic drawing of back-scattered electron detector for flat and stereo observations (fabricated by Alton Electronics, Inc.) with the electron microprobe

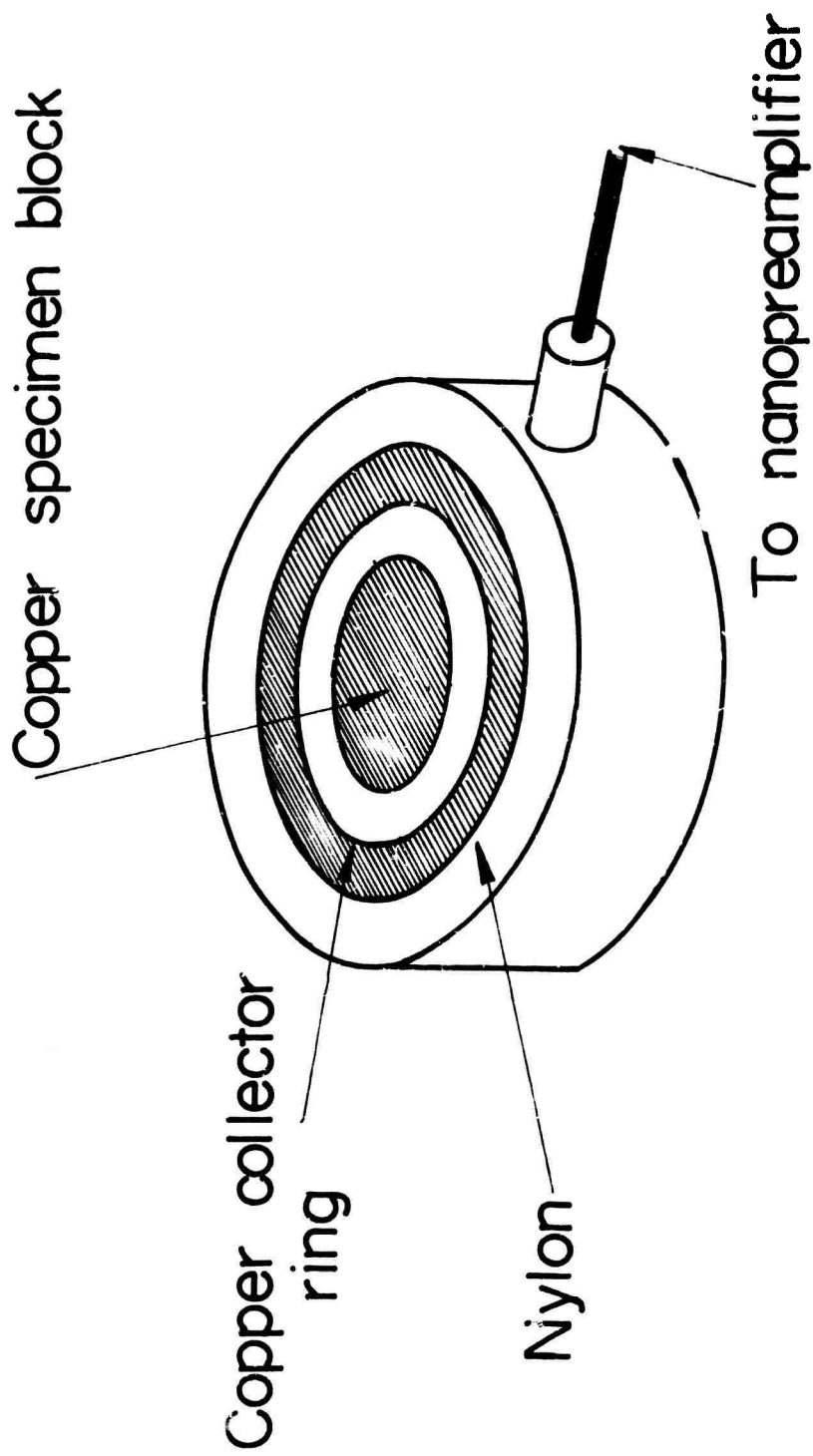


Fig. 1 Schematic drawing of back-scattered electron detector for flat and stereo observations (fabricated by Alton Electronics, Inc.) with the electron microprobe.

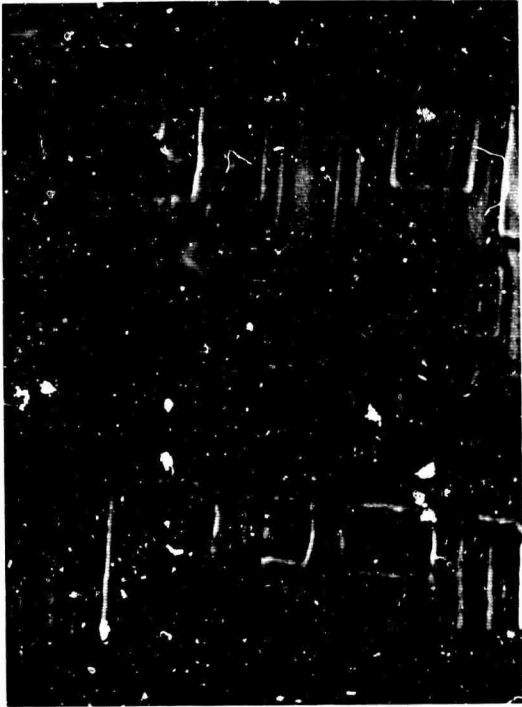


Fig. 2 The specimen current intensity from integrated circuit chip. Area 300 x 300 microns.

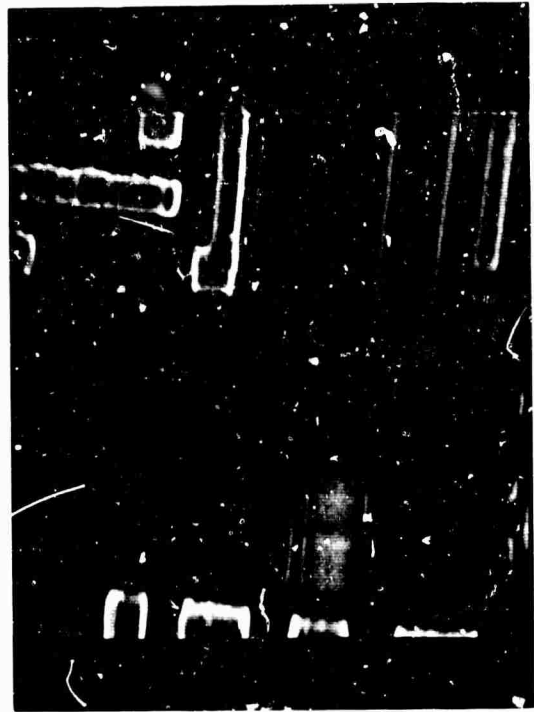


Fig. 3. A secondary electron image (flat) 67-1/2 volt bias from an integrated circuit chip. Area 300 x 300 micron.

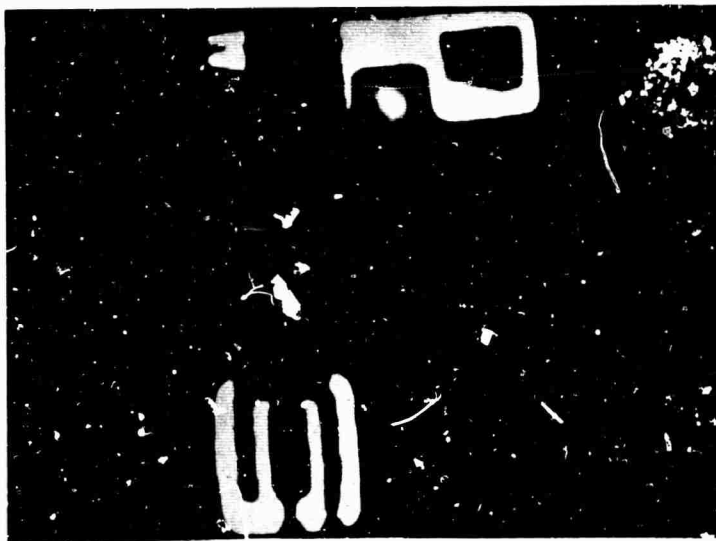


Fig. 4 Secondary electron image of the microcircuit biased to 500 MV (after H. R. Potts⁵).



Fig. 5 Secondary electron image of the same microcircuit biased to 1,000 MV (after H. R. Potts⁵).

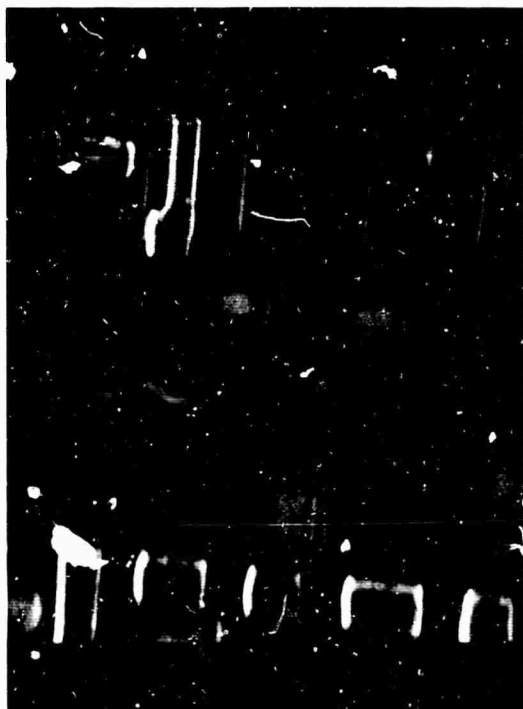


Fig. 6 Secondary electron image in the stereo mode, 67-1/2 volt bias. Area same as Fig. 4



Fig. 7 Secondary electron image using large collector plate, note distorted image by increased image intensity. Area same as Fig. 4.



Fig. 8 Solder joint viewed with secondary electrons in stereo mode, 6 volt bias. Area 300 x 300 microns

C. MAGNETIC FILM LABORATORY
(J.K. Watson; assisted by R.G. Singh)

Two aspects of the magnetic film laboratory are currently being developed: the vacuum deposition facility and instrumentation for preliminary evaluation of film performance. The immediate objective is to be able to fabricate films and to make a preliminary evaluation of their performance. It is intended that an initial rough characterization of performance would be used two ways: first, as a "bootstrap" to guide the establishment of deposition procedures; but more important, as a mechanism of establishing our first experimental interaction with the metallurgy branch of the research team. Such an interaction is necessary to the attainment of our long-range objective: the correlation of electrical performance measurements with metallurgical structural properties.

Laboratory Facilities

Two aspects of the magnetic film laboratory are currently being developed: the vacuum deposition facility and some instrumentation for preliminary evaluation of film performance. Most of the major pieces of equipment described below were bought from other funds. However their incorporation into a film research facility is supported by THEMIS.

Since the time of the original proposal (May 1, 1967) our Varian vacuum system has arrived, has been debugged, and has met acceptance tests. Its 500 l/sec ion pump plus titanium sublimation pump, after an appropriate system bakeout schedule, takes the base pressure to the low 10^{-9} torr range although the system has a glass bell-jar with elastomer L-gasket seal. (The system has metal flange seal capability by replacing the bell-jar, for investigations which may require even higher vacuum environment.) Some basic performance levels have been established experimentally for the empty system; bake-out provisions have been made; a work-coil configuration for induction heater evaporation has been developed, with RF and water feedthru; the thermal design of the crucible and holder has been tested satisfactorily using a 1 KW RF power source which was available here. One KW was just insufficient to permit evapo-

ration; a 5 KW unit is on order. These tests also suggest that, after appropriate pre-heating of the material, it may be possible to maintain a base pressure in the range of 10^{-8} torr during evaporation. The maintenance of such a low pressure would meet our objectives very well, especially in conjunction with the fast evaporation rate expected from the 5 KW RF drive.

The design is completed of substrate heater and holder, shutter mechanism, and internal support structure. Our model shop is fabricating them. A substrate temperature controller has been ordered. A quartz crystal oscillator type of film thickness monitor and deposition rate controller has been ordered. A non-magnetic bell-jar hoist, external coil forms (for generating the anisotropy-inducing magnetic field), and power supply have all been specified and are being build in our model shop.

Several instruments for magnetic film performance measurement are being developed. There has been developed electrically an instrument for the measurement of flux-reversal losses (B-H loop). There has just become operational a pulsed-field system, for measuring flux-switching in the intermediate speed range of about 1/2 microsecond. The latter measurements have been previously found to vary tremendously with film parameters; furthermore such pulsed instrumentation is easily adapted to other applications such as dispersion measurements or such as domain wall mobility measurements. We are presently attempting our first serious use of this new system. The environment for these measurements is provided by a cube-coil array for the local cancellation of earth's field, designed and built previously. Current regulation for the cube coils reduces the short-term drift to less than 5 millioersted.

Under a related program, preliminary efforts are being made toward the development of a pulsed stripline system for the measurement of flux reversal in the low nanosecond range.

Optical benches, polarizers and lenses are being assembled into a Kerr magneto-optical setup; the related coils and alignment jigs are being developed here. Film thickness will be checked optically using a standard Nomarski attachment for our Reichert microscope. Some preliminary feasibility studies are also in process, exploring the practicability of applying various techniques of optical fringe measurements to the observation of film structural details.

Dr. Dove has put into preliminary operation a high resolution Kerr-effect scanning system to aid in the film structural determinations.

VII. DISCUSSION

The first semiannual period has seen much progress made toward the achievement of the research goals outlined in Section I. The recruitment and training of staff has proceeded well, as has the development of laboratories for: noise studies, device fabrication, magnetic film fabrication and evaluation, and the measurement of structural parameters. From these laboratories have already emerged technical findings - some detailed and conclusive, others as yet tentative and preliminary. The dielectrics laboratory, coupled with the facilities for electron microscopy and x-ray analysis, have, in particular, yielded significant results.

The next semiannual period will see the arrival and installation of the Hall magnet and associated equipment, and of the optical equipment for lifetime measurements. This equipment will enable the securing of data relevant to such electronic and quantum parameters as: collision and capture cross sections, energy levels and their degeneracies, band structure, and mobility and diffusivity. This data, coupled with electronic measurements made with the facilities now available, will be correlated with data on material structure, some of which has begun to be gathered during this period. Further correlation will be sought with radiation studies. This materials research will both interact with collateral device studies and will be guided by them.

This is the plan of the research. The progress made thus far supports our view that we are proceeding toward the general objective: the establishment at the University of Florida of a center of competence in unconventional solid-state materials and devices.

Security Classification

14. KEY WORDS	LINK A		LINK B		LINK C	
	ROLE	WT	ROLE	WT	ROLE	WT
Degenerate Semiconductors Surface Defects in Diamond Cubic Materials Einstein Relation Noise Magnetic films Semiconducting Glasses Glass-Ceramic Dielectrics Irradiation of Glasses						